Magnetic anisotropy of Fe and Co ultrathin films deposited on Rh(111) and Pt(111) substrates: An experimental and first-principles investigation

Anne Lehnert,[1] Samuel Dennler,[2] Piotr Błoński,[3] Stefano Rusponi,[1] Markus Etzkorn,[1] Géraud Moulas,[1] Peter Bencok,[4] Pietro Gambardella,[5,6] Harald Brune,[1] and Jürgen Hafner[3]

[1]*Institute of Condensed Matter Physics, Ecole Polytechnique Fédérale de Lausanne (EPFL), CH-1015 Lausanne, Switzerland*

[2]*Laboratoire des Colloïdes, Verres et Nanomatériaux, Université de Montpellier II, F-34095 Montpellier, France*

[3]*Fakultät für Physik and Center for Computational Materials Science, Universität Wien, Sensengasse 8/12, A-1090 Wien, Austria*

[4]*European Synchrotron Radiation Facility, Boîte Postale 200, F-38043 Grenoble, France*

[5]*Centre d'Investigacions en Nanociència i Nanotecnologia, ICN-CSIC, UAB Campus, E-08193 Bellaterra, Spain*

[6]*Institució Catalana de Recerca i Estudis Avançats (ICREA), E-08100 Barcelona, Spain*

(Received 12 May 2010; revised manuscript received 15 July 2010; published 3 September 2010)

We report on a combined experimental and theoretical investigation of the magnetic anisotropy of Fe and Co ultrathin layers on strongly polarizable metal substrates. Monolayer (ML) films of Co and Fe on Rh(111) have been investigated *in situ* by x-ray magnetic circular dichroism (XMCD), magneto-optic Kerr effect, and scanning tunneling microscopy. The experiments show that both magnetic adlayers exhibit ferromagnetic order and enhanced spin and orbital moments compared to the bulk metals. The easy magnetization axis of 1 ML Co was found to be in plane, in contrast to Co/Pt(111), and that of 1 ML Fe out of plane. The magnetic anisotropy energy (MAE) derived from the magnetization curves of the Fe and Co films is one order of magnitude larger than the respective bulk values. XMCD spectra measured at the Rh $M_{2,3}$ edges evidence significant magnetic polarization of the Rh(111) surface with the induced magnetization closely following that of the overlayer during the reversal process. The easy axis of 1–3 ML Co/Rh(111) shows an oscillatory in-plane/out-of-plane behavior due to the competition between dipolar and crystalline MAE. We present a comprehensive theoretical treatment of the magnetic anisotropy of Fe and Co layers on Rh(111) and Pt(111) substrates. For free-standing hexagonally close-packed monolayers the MAE is in plane for Co and out of plane for Fe. The interaction with the substrate inverts the sign of the electronic contribution to the MAE, except for Fe/Rh(111), where the MAE is only strongly reduced. For Co/Rh(111), the dipolar contribution outweighs the band contribution, resulting in an in-plane MAE in agreement with experiment while for Co/Pt(111) the larger band contribution dominates, resulting in an out-of-plane MAE. For Fe films however, the calculations predict for both substrates an in-plane anisotropy in contradiction to the experiment. At least for Fe/Pt(111) comparison of theory and experiment suggests that the magnetic structure of the adlayer is more complex than the homogenous ferromagnetic order assumed in the calculations. The angular momentum and layer-resolved contributions of the overlayer and substrate to the MAE and orbital moment anisotropy are discussed with respect to the anisotropic hybridization of the 3*d*, 4*d*, and 5*d* electron states and vertical relaxation. The role of technically relevant parameters such as the thickness of the surface slab, density of *k* points in the Brillouin zone, and electron-density functionals is carefully analyzed.

DOI: 10.1103/PhysRevB.82.094409 PACS number(s): 75.30.Gw, 75.75.−c, 71.15.Mb, 78.70.Dm

I. INTRODUCTION

The potential application in magnetic or magneto-optic data storage devices has motivated intense research efforts directed toward an improved understanding of the fundamental properties of magnetic nanostructures. To increase the density of information per square inch is of course one of the central goals. In current devices, one bit of information is stored in a few hundred single-domain particles or grains, and the ultimate limit of storage density will be achieved if one bit is stored per grain. In order to avoid loss of information through thermally activated magnetization reversal, the magnetic anisotropy energy (MAE) must be at least 1.2 eV/grain. To reduce the size per bit requires therefore an increased MAE per atom. In addition, in order to reduce dipolar magnetic interactions between neighboring bits, the easy axis of magnetization has to be perpendicular to the plane of the storage disk. A high magnetization density of the recording medium is required to remain within the range of technologically realistic writing fields. Extensive efforts have been devoted to the development of new materials meeting these requirements.[1–4]

Magnetic anisotropy is a relativistic effect promoted by the spin-orbit coupling (SOC). A high magnetization density requires a large magnetic moment per atom. Large moments are found among the magnetic 3*d* metals Fe, Co, and Ni while spin-orbit coupling is strongest among the heavy 4*d* or 5*d* elements (which are, however, nonmagnetic). Hence bimetallic systems consisting of ferromagnetic 3*d* elements and heavy 5*d* elements seem to offer a viable route to improve both the saturation magnetization and the MAE. In addition, the crystalline structure plays a decisive role. In the cubic 3*d* ferromagnets the leading contribution to the MAE is fourth order in the SOC matrix element, leading to an MAE on the order of a few microelectron volts per atom. In layered FePt compounds with a tetragonal $L1_0$ structure the leading contribution is second order in the SOC and the MAE may reach nearly 1 meV/atom.

In ultrathin films, supported wires or nanostructures the characteristic dimensions approach a few interatomic dis-

tances. In this case, the electronic structure of the magnetic material is increasingly dependent on the hybridization with the substrate. A very striking example is provided by the giant MAE of 9.3 ± 1.6 meV/atom reported for isolated Co atoms on a Pt(111) substrate.[5] Arrays of parallel atomic chains of Co grown along the steps of a Pt(997) vicinal surface have been prepared by Gambardella *et al.*[6,7] Spin and orbital moments and the MAE were determined using x-ray adsorption spectroscopy (XAS) and x-ray circular magnetic dichroism (XCMD). Monatomic wires (Ref. 8) show superparamagnetic behavior and below a blocking temperature long-range ferromagnetic order develops due to a large MAE of 2.0 ± 0.2 meV/atom. If the entire Pt(997) surface is covered by a monolayer (ML) Co film, the MAE drops to 0.14 ± 0.01 meV/atom. The magnetic properties of atomically thin Fe layers on flat and vicinal Pt surfaces have been investigated by Repetto *et al.* (Ref. 9). Very recently, the magnetic properties of Fe, Co, and Fe-Co alloy monolayers on a flat Pt(111) surface have been measured by Moulas *et al.*.[10] The MAE is essentially the same as for the vicinal surface. The orbital moment of the Co atoms shows the same variation as the MAE with the dimensionality of the nanostructure, namely, $\mu_L = 1.1\ \mu_B$, $0.68\ \mu_B$, and $0.31\ \mu_B$ for an isolated adatom, a monatomic wire, and a monolayer, respectively.

These experimental results have inspired a number of theoretical studies based on spin-density-functional theory (SDFT) (Refs. 5 and 10–21) covering systems of different dimensionality. SDFT calculations of the MAE necessitate a number of approximations: choice of the exchange-correlation functional [local or semilocal (gradient-corrected)], geometry of the adsorbate/substrate complex (ideal bulklike geometry or full relaxation), full potential, or atomic-sphere approximation, MAE determined by total-energy (TE) differences or via the "magnetic force theorem (FT)." Very recently, two of us have attempted to assess the validity of these approximations at the example of the MAE of isolated Co and Fe atoms on a Pt(111) substrate.[21]

While most experimental and theoretical studies have concentrated on nanostructures supported on Pt substrates, less attention has been paid to systems supported on surfaces of the 4*d* metals Pd or Rh.[22–26] The influence of these substrates on the properties of magnetic nanostructures is of particular interest for the following reasons. Because of a low *d*-band width compared to the 5*d* metals, the 4*d* metals Pd and Rh are much closer to the onset of magnetism. For small clusters[27,28] and ultrathin films[29,30] of Rh and Pd ferromagnetic ordering has been predicted. Experimental confirmation of these predictions comes from Stern-Gerlach experiments of small Rh clusters[31] and magnetization measurements on fine Pd particles[32] demonstrating their magnetic heterostructure: the shell orders ferromagnetically whereas the core remains paramagnetic. Both Pd and Rh are highly polarizable. It is well known that an isolated magnetic impurity in a Pd matrix displays a "giant" effective magnetic moment composed by the magnetic moment of the impurity moment plus a large induced magnetization cloud.[33,34] Large induced moments on the Pd atoms have also been reported for layered FePd compounds with a $L1_0$ structure.[35]

In this paper we present the results of combined experimental and theoretical investigations of the magnetic properties of Fe and Co monolayers on Rh(111) and Pt(111) substrates. The choice of Rh(111) as substrate is of special interest because (i) the high spin-orbit coupling constant of Rh may give rise to very large anisotropy energies, (ii) an induced magnetic moment in the Rh atoms close to the interface is expected,[36–38] and (iii) the magnetic properties of 1 ML Co(Fe) grown on Rh(111) are difficult to predict. Tomaz *et al.*[37,38] studied multilayers of Fe/Rh(001) and Co/Rh(001) finding Rh moments up to 1 μ_B strictly limited to the interface. In contrast, Dennler *et al.*[36] predicted that Co monolayers adsorbed on top or slightly below a Rh(111) surface induce a long-range oscillatory magnetic polarization of the substrate. Fe overlayers on Rh(001) were studied by photoelectron spectroscopy and x-ray magnetic circular dichroism (XMCD) finding suppression of ferromagnetic order up to 3 ML.[39,40] *Ab initio* calculations for 1 ML Fe/Rh(001) gave evidence of an energetically favored antiferromagnetic (AFM) ordering in the Fe layer caused by a very strong adlayer/substrate hybridization.[41] Likewise a FeRh compound with the CsCl crystal structure is AFM below 370 K with $m_{\mathrm{Fe}} = \pm 3\ \mu_B$ while no considerable moment for Rh is observed.[42] However, in a triangular magnetic adlayer adsorbed on the Rh(111) surface the threefold symmetry would lead to a frustrated AFM so that the actual magnetic ground state is difficult to predict. A pseudomorphic Fe monolayer grown on Rh's 5*d* complement Ir(111) exhibits a novel noncollinear magnetic structure with 15 atoms per unit cell.[43]

For the system Co on Rh(111) the focus is set on the easy axis of magnetization. Thin Co layers are in general ferromagnetically ordered but the choice of the substrate influences strongly the easy magnetization axis. A 1.5 ML Co/Cu(100) film shows in-plane anisotropy,[39,44] whereas 1 ML Co/Pt(111),[8,9] 2 ML Co/Pd(111),[23] and >1.5 ML Co/Rh(111) (Ref. 45) films have an easy magnetization direction perpendicular to the surface. A rather complex spin-reorientation transition was observed for thin Co films on Ru(0001) having an equal in-plane lattice constant as Rh(111) (2.70 Å for Ru and 2.69 Å for Rh) but a different electronic structure in the atomic ground state ($4d^7$ for Ru and $4d^8$ for Rh). 1 ML Co/Ru(0001) has an in-plane easy axis of magnetization, rotating out of plane for 2-ML-thick films[46] while from 3 ML Co on the easy axis is again in plane.

Fe and Co monolayers on Rh(111) substrates have been investigated using XAS, XMCD, magneto-optical Kerr effect (MOKE) experiments, and scanning tunneling microscopy (STM) measurements. We found ferromagnetic order in both the Fe and Co monolayers. One monolayer of Fe is out of plane with a small MAE. Co is in plane for 1 ML, with a larger MAE than Fe. 2 ML Co/Rh(111) are out of plane and 3 ML Co/Rh(111) again in plane. We take advantage of the element specificity of XMCD to show that Rh is polarized by the magnetic adlayer.

Ab initio spin-density-functional calculations have been performed for free-standing hexagonally close-packed (hcp) Co and Fe monolayers and for layers adsorbed pseudomorphically on Rh(111) and Pt(111) substrates. The calculations have been performed using a gradient-corrected exchange-correlation functional and for fully relaxed monolayers and adlayer/substrate complexes. The Hellmann-Feynman forces

acting on the atoms have been used to perform a structural optimization of the adsorbate/substrate complex. The MAE has been calculated as the difference in the total energies from self-consistent calculations for in-plane and out-of-plane magnetization but the magnetic force theorem which permits to approximate the MAE by the difference in the band energies from nonself-consistent calculations has been used to decompose the MAE into contributions from the magnetic adlayer and from the induced magnetic moments in the top layers of the substrate. This approach allows to achieve a deeper understanding of the mechanisms determining the magnetic anisotropy in low-dimensional systems combining the high magnetic moments of low-coordinated atoms with a support providing strong spin-orbit coupling.

II. EXPERIMENT

The x-ray experiments were performed at the ID08 beamline of the European Synchrotron Radiation Facility in Grenoble providing an ultrahigh-vacuum (UHV) chamber for *in situ* sample preparation and characterization using synchrotron light. In this chamber the Rh(111) substrate was prepared by repeated cycles of Ar-ion sputtering (1.3 keV at 300 K), followed by annealing at 800 K in an oxygen atmosphere of $P_{O_2}=5\times10^{-8}$ mbar and final annealing at 1000 K. Surface cleanliness was confirmed by Auger electron spectroscopy and XAS. Co and Fe were deposited by atomic beam epitaxy from high-purity rods (99.995%) at a sample temperature of 10 K. Low-temperature deposition, where diffusion is inhibited, leads to granular films as discussed in Ref. 10. During deposition the pressure was below 1×10^{-10} mbar. The deposition rate determined by STM and XAS was 1×10^{-3} ML/s and 5×10^{-4} ML/s for Co and Fe, respectively. XAS were taken in the total electron yield (TEY) mode using $99\pm1\%$ circularly polarized light while the sample was magnetized by a variable magnetic field up to ±5 T. The magnetic field is collinear with the photon beam and its polar angle with respect to the surface normal θ has been varied in order to address magnetic anisotropy. The XMCD signal is the difference in XAS recorded for parallel μ_+ and antiparallel μ_- alignment of the photon helicity with the applied magnetic field **H**.

MOKE measurements were carried out using an experimental setup combining STM and MOKE and described in Ref. 47. In this chamber the Rh(111) crystal was prepared in a similar way as for the synchrotron experiments with the only difference of a final annealing up to $T=1400$ K. Two different types of films were grown for MOKE experiments: granular and continuous films. The deposition rates have been adjusted to the ones of the synchrotron experiments and the pressure during deposition was $p<2\times10^{-10}$ mbar. Granular films were deposited at $T=50$ K and continuous films were grown in a temperature range between 50 and 95 K followed by annealing at $T=300$ K for 5 min. Polar and transverse MOKE were measured at different temperatures and the morphology of the film was characterized by means of STM. Note that final film morphologies and their magnetic properties of the continuous films were independent of the deposition temperature in the interval given above.

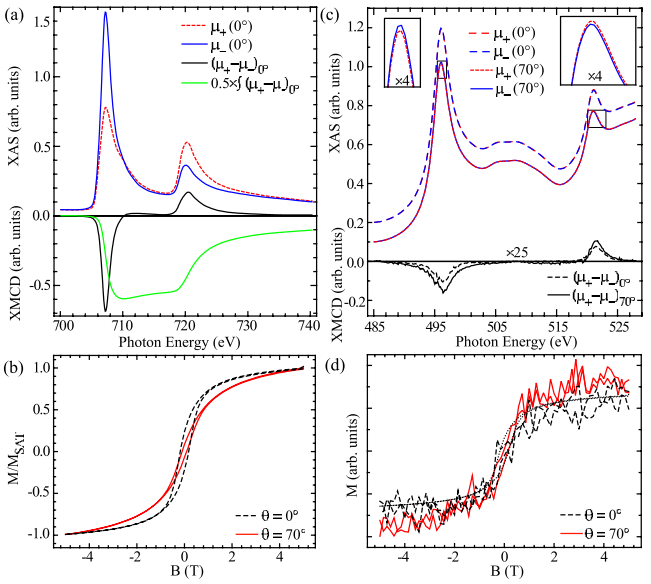

FIG. 1. (Color online) XAS and XMCD spectra for 0.80 ML Fe/Rh(111). (a) Background subtracted XAS taken at the Fe $L_{2,3}$ edges at $T=10$ K at $\theta=0°$ and resulting XMCD spectrum. The green line is the integrated XMCD spectrum. (b) Magnetization curves at $\theta=0°$ and 70° measured at $T=10$ K by taking the peak height of the L_3 XMCD intensity at 707.1 eV divided by the pre-edge intensity at 704.0 eV as a function of the applied magnetic field. (c) XAS and XMCD spectra, the latter has been magnified by a factor of 25, of the Rh $M_{2,3}$ edges measured for a 0.56 ML Fe film at $\theta=0°$ and 70°. The spectra at 70° have been normalized to the pre-edge M_3 intensity and offset for clarity. The zooms into the $M_{2,3}$ edge intensity (insets) evidence the polarization dependence. (d) Magnetization curves of 0.80 ML Fe/Rh(111) at $\theta=0°$ and 70° measured at $T=10$ K by taking the peak height of the M_3 XMCD intensity at 496.2 eV divided by the pre-edge intensity at 491.0 eV as a function of the applied magnetic field. The dotted curve indicates the Fe magnetization curve at $\theta=0°$ shown in (b).

III. XAS AND XMCD STUDY OF 1 ML GRANULAR FILMS

We investigated the magnetic and electronic properties of granular films and of the substrate by taking XAS at the $L_{2,3}$ edges of Fe and Co and the $M_{2,3}$ edges of the Rh(111) substrate. The orbital moment L and effective spin magnetic moment $S_{eff}=S+7D$ with S the spin and D the intra-atomic spin dipole moment of Co and Fe were determined along the easy magnetization axis of the saturated sample using the XMCD sum rules.[48–50] Out-of-plane vs in-plane magnetic behavior was investigated by taking XAS for normal ($\theta=0°$) and grazing ($\theta=70°$) incidence. MOKE in polar and transverse geometry of granular and continuous films confirm the easy axis and anisotropic behavior inferred from XMCD.

A. Magnetic moments of Fe and Co

The results for 0.80 ML Fe/Rh(111) are reported in Fig. 1. From the hysteresis curves shown in (b) we infer an easy axis of magnetization along the surface normal and we note that saturation is reached at both angles. Applying the sum rules to the XAS and XMCD spectra measured at the Fe $L_{2,3}$

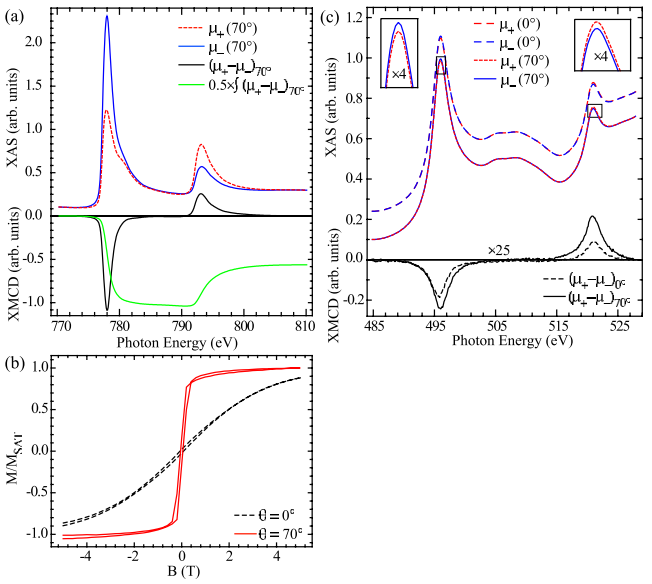

FIG. 2. (Color online) XAS and XMCD spectra for 1.25 ML Co/Rh(111). (a) Background subtracted XAS taken at Co $L_{2,3}$ edges at $T=10$ K at $\theta=70°$ and resulting XMCD spectrum. The green line is the integrated XMCD spectrum. (b) Magnetization curves at $\theta=0°$ and 70° measured at $T=10$ K by taking the peak height of the L_3 XMCD intensity at 778.0 eV divided by the pre-edge intensity at 774.5 eV as a function of the applied magnetic field. (c) XAS and resulting XMCD spectra of Rh $M_{2,3}$ edges shown with a $\times 25$ magnification and measured across the 1.25 ML Co film at $\theta=0°$ and 70°. The spectra at 70° have been normalized to the pre-edge M_3 intensity and offset for clarity. Zooms into the $M_{2,3}$ edge intensity (insets) evidence the difference of the μ_+ and μ_- XAS.

edges along the easy axis we obtain $L/h_d = 0.05 \pm 0.01$ μ_B/atom and $S_{eff}/h_d = 0.74 \pm 0.03$ μ_B/atom for Fe/Rh(111). For the number of d holes we take our calculated value $h_d=3.9$, leading to an orbital magnetic moment of $L=0.21 \pm 0.04$ μ_B/atom and $S_{eff}=2.89 \pm 0.12$ μ_B/atom. In the case of uniaxial anisotropy, angle-dependent XMCD measurements allow the separation of D and S for saturated samples.[51] S is assumed to be angle independent while D varies as

$$D_\theta = D_{0°}\left(\cos^2\theta - \frac{1}{2}\sin^2\theta\right). \quad (1)$$

The measurement at $\theta=70°$ yields $S+7D_{70°} = 2.71 \pm 0.12$ μ_B/atom resulting in $7D_{0°}/S=0.05$, in very good agreement with earlier DFT calculations,[52] and a spin magnetic moment of $S=2.76 \pm 0.16$ μ_B/atom.

A granular 1.25 ML Co/Rh(111) film has an in-plane easy magnetization axis according to the magnetization loop shown in Fig. 2(b). The corresponding XAS taken at the Co $L_{2,3}$ edges at $\theta=70°$, the XMCD spectrum, and its integral are shown in Fig. 2(a). From the sum rules we obtain $L/h_d = 0.12 \pm 0.02$ μ_B/atom and $S_{eff}=0.74 \pm 0.03$ μ_B/atom. Using $h_d=2.8$ from our calculation we obtain an orbital magnetic moment of $L=0.34 \pm 0.06$ μ_B/atom and $S_{eff} = 2.07 \pm 0.08$ μ_B/atom. The spin magnetic moment cannot be separated in this case because the hard axis is not saturated. Assuming a magnetic dipole contribution of $7D/S = 0.05$ as in the case of Fe, we obtain $S = 1.97 \pm 0.08$ μ_B/atom. The DFT calculations described below yield a magnetic moment in the Co adlayer of 1.96 μ_B which is in very good agreement with our experimental results.

B. Induced polarization

Rh is known to be a nonmagnetic, although highly polarizable, Stoner enhanced material. In order to investigate a possible induced magnetic polarization of the substrate and its influence on the magnetism of the film/substrate complex, we compared XAS acquired on the clean and on the Fe, respectivly, Co covered surface. We measured the $M_{2,3}$ absorption edges of the pristine Rh(111) substrate at $T=10$ K with $B=\pm 5$ T and observe no magnetic polarization. We took special care to average over a large number of absorption spectra (minimum 10) to improve the signal-to-noise ratio. XAS recorded after Fe deposition are displayed in Fig. 1(c). A zoom in the absorption intensities (see insets) evidences a small difference for XAS acquired with positive and negative x-ray helicity. The corresponding XMCD signal is shown in the lower part with a $\times 25$ magnification. By comparing the sign of the dichroism of Rh and Fe we conclude that the Rh moments are ferromagnetically aligned with the Fe moments. We cannot apply the sum rules mainly for two reasons: (i) the measured x-ray absorption intensity integrates over several Rh layers of which only a few carry a magnetic moment and (ii) due to saturation effects, which are important for bulk samples,[53] the TEY signal does not reflect the true x-ray adsorption coefficient. Saturation effects arise when the x-ray penetration depth λ_x becomes comparable to the electron escape depth which is about 20 Å. At the $L_{2,3}$ absorption edges of $3d$ metals λ_x is only 200 Å which efficiently reduces the incident x-ray intensity at sampling depth contributing to the TEY. Moreover, the x-ray penetration depth depends on the incidence angle making the XAS taken at grazing incidence ($\theta=70°$) more sensitive to the surface layers than XAS taken at normal incidence ($\theta=0°$). Thus, the larger XMCD signal obtained for grazing incidence is due to an increased sensitivity to the induced Rh magnetization being limited to a few Rh layers close to the interface. Despite the small XMCD signal we managed taking magnetization curves of the Rh substrate as shown in Fig. 1(d). For comparison, the dotted line represents the scaled magnetization curve for the Fe adlayer taken at $\theta=0°$ indicating a coherent switching behavior of adlayer and induced magnetization in the substrate.

Similarly, we measured XAS of the $M_{2,3}$ edges of Rh buried under a Co monolayer as shown in Fig. 2(c). The small difference of the XAS acquired with μ_+ and μ_- is shown in the insets. The resulting XMCD spectrum is shown underneath with a $\times 25$ magnification. Again, we conclude from the sign of the XMCD spectra of Co and Rh that the magnetic moments of both elements are ferromagnetically aligned, however saturation effects prevent an estimation of the Rh magnetic moment.

C. Magnetic anisotropy

The anisotropy energy can be calculated from the saturated magnetization curves using[8,55]

$$E_a = \frac{\int_0^{M_{\text{sat}}} B dM_{\theta_1} - \int_0^{M_{\text{sat}}} B dM_{\theta_2}}{\sin^2(\theta_1 - \theta_2)}. \quad (2)$$

The total magnetic moment in the integrand is the effective moment per Fe or Co atom given by $M=S+L+m_{\text{Rh}}$, where S and L stand for the spin and orbital moment of the magnetic adatoms and m_{Rh} represents the total magnetic moment induced on Rh sites per Fe or Co atom. Since m_{Rh} is not known experimentally, we will calculate lower bounds of E_a using $m_{\text{Rh}}=0$.

The magnetization curves of Fe/Rh(111) are saturated for both angles. Thus we can readily calculate E_a using Eq. (2) and obtain an out-of-plane anisotropy of $E_a > (0.08 \pm 0.01)$ meV/Fe atom.

For Co the shape of the magnetization curve recorded at $\theta=70°$ is nearly square suggesting the easy magnetization axis to be in plane. Equation (2) yields $E_a < -0.31$ meV/Co atom after extrapolation of the hard-axis magnetization curve to saturation. Dennler *et al.*[36] calculated an induced moment of 0.4 μ_B in the Rh top layer. According to Eq. (2), the MAE per Co atom would thus increase by 0.06 meV, giving 0.06 meV/Co atom to the MAE giving $E_a=-(0.37 \pm 0.05)$ meV/Co atom.

IV. MOKE OF 1 ML GRANULAR AND CONTINUOUS FILMS

We investigated granular and continuous monolayer films with MOKE in polar and transverse geometry to probe out-of-plane vs in-plane magnetization as a function of magnetic field. The granular films consist of clusters of mostly single atomic height with a broad size distribution.[10] For a coverage of 0.90 ± 0.10 ML deposited at $T=60$ K we infer from STM images for Fe and Co a mean island size of 70 atoms; less than 0.03 ML are found in the second layer. For granular Fe films we observe at $T=60$ K a line of constant slope for polar Kerr and no signal for transverse Kerr (not shown) typical for superparamagnetic Fe clusters with out-of-plane anisotropy and above the blocking temperature. Annealing at $T=300$ K for 5 min leads to the formation of a continuous film with long-range ferromagnetic order. Figure 3 shows that a continuous Fe film of (1.00 ± 0.05) ML on Rh(111) exhibits an s-shaped hysteresis loop for polar Kerr with a coercive field of 20 mT and only a very weak transverse Kerr signal. The maximum field amplitude of $B_{\text{max}}=315$ mT is not sufficient to saturate the sample in the easy direction. STM images of the first monolayer showed no evidence for surface partial dislocation lines which would be characteristic for surface stress relaxation [Fig. 3(c)] and thus we conclude pseudomorphic growth for the Fe monolayer.

Granular Co films display a polar and transverse MOKE signal similar to the continuous (1.00 ± 0.05) ML film shown in Figs. 4(a) and 4(b). The hysteresis loop taken in transverse geometry evidences an in-plane easy magnetization axis. The coercive field is $\mu_0 H_c = 7 \pm 1$ mT. The shape of this curve is not the expected square shape and resembles the one reported equally for transverse MOKE by Lee *et al.*[54] An STM image of the continuous film is shown in Fig. 4(c).

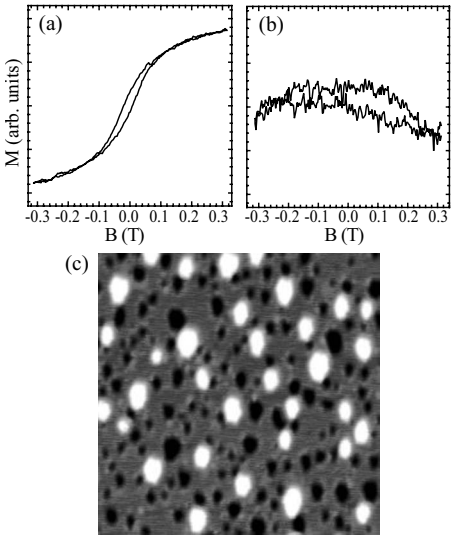

FIG. 3. 1.00 ± 0.05 ML Fe/Rh(111) deposited at $T=53$ K and annealed at 300 K for 5 min. (a) Polar and (b) transverse MOKE measured at $T=65$ K. (c) STM image measured at $T=65$ K; 500 $\times 500$ Å^2, $V_t=-0.1$ V, and $I_t=5$ nA.

Differently from Fe, the Co film shows bright lines with an apparent height of (5.5 ± 0.5) pm on the otherwise flat monolayer. These lines are interpreted as surface partial dislocations separating hcp from fcc stacking regions of the adlayer with respect to the substrate. The fraction of the monolayer imaged with constant apparent height is 82 ± 3 %. We conclude that this fraction of the atoms are on pseudomorphic sites. This is a lower bound since tip convolution slightly widens the line defects.

The structural properties of the Fe and Co films on Rh(111) are similar to those of Fe and Co on Pt(111) discussed in Ref. 10. However, the magnetic properties are

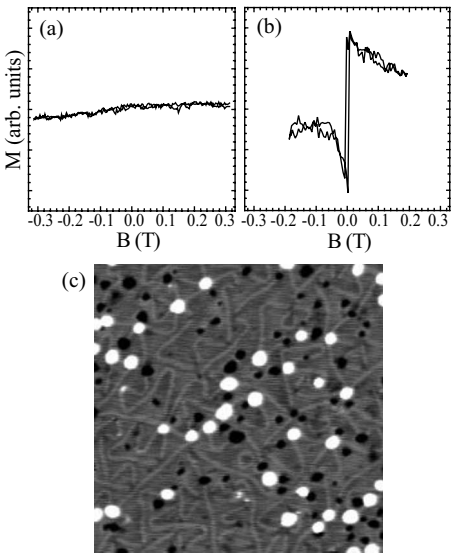

FIG. 4. 1.00 ± 0.05 ML Co/Rh(111) deposited at $T=60$ K and annealed at 300 K for 5 min. (a) Polar and (b) transverse MOKE measured at $T=60$ K. (c) STM image measured at $T=60$ K; 500 $\times 500$ Å^2, $V_t=-0.8$ V, and $I_t=5$ nA.

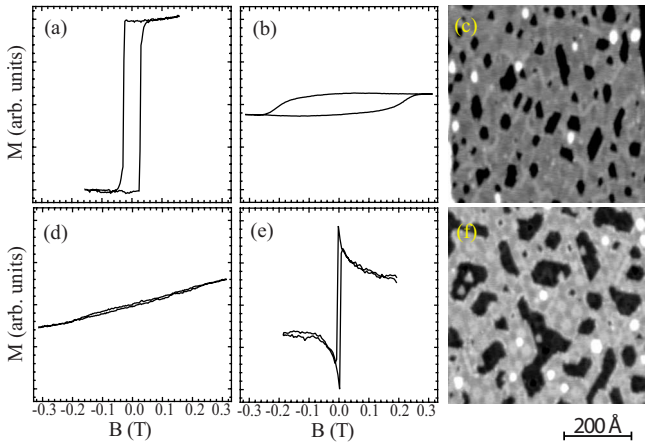

FIG. 5. (Color online) MOKE spectra and STM images for Co/Rh(111) films of [(a)–(c)] (1.8 ± 0.1) ML and [(d)–(f)] (2.7 ± 0.2) ML thickness. (a) Polar and (b) transverse MOKE. (c) STM image evidencing dislocation lines in the second layer; $V_t=-0.01$ V and $I_t=2$ nA. (d) Polar and (e) transverse MOKE. (f) STM image evidencing a trigonal dislocation network in the third monolayer; $V_t=-0.01$ V and $I_t=1$ nA. The films were obtained by successively depositing 1 ML at $T=60$ K and annealing at $T=300$ K for 5 min. The MOKE and STM measurements are performed at $T=60$ K.

quite different. Co/Rh(111) is in plane whereas Co/Pt(111) is out of plane. For Fe/Pt(111) we found in Ref. 10 a reduced spin moment of 1.2 ± 0.2 μ_B/atom which was tentatively explained by assuming a complex magnetic structure with prevalent antiferromagnetic order as recently observed for one monolayer Fe/Ir(111).[43] The spin moment for 1 ML Fe/Rh(111) is $S=2.76\pm0.16$ μ_B/atom from which we can safely conclude that the Fe film orders ferromagnetically.

V. EXPERIMENTAL RESULTS OF CONTINUOUS Co AND Fe MULTILAYERS

We have investigated the evolution of the magnetic properties as a function of film thickness. Fe/Rh(111) films have out-of-plane easy axis up to 4 ML from where on it turns toward in plane. This spin-reorientation transition is completed at 6 ML and due to the dipolar term dominating the interface magnetocrystalline out-of-plane anisotropy at high coverage.

The results for continuous Co films of 1.8 ± 0.1 and 2.7 ± 0.2 ML thickness are presented in Fig. 5. In the second layer the lattice mismatch leads to the formation of surface partial dislocation lines similar to those observed in the first layer. In the third layer loops of partial surface dislocations are observed similar to those reported for 3 ML Ag/Pt(111),[56] for 2 ML Cu/Pt(111),[57] and for 3 ML Cu/Ru(0001).[58] Polar and transverse Kerr spectra evidence a twofold spin-reorientation transition as a function of film thickness. The easy axis turns from in plane for 1 ML to out of plane for 2 ML and back to in plane for ≥ 3 ML. The residual in-plane signal of the 1.8 ML sample is attributed to the coexistence of the second with the first and third monolayer. Similarly, the residual out-of-plane signal for 2.7 ML originates from the coexisting second layer. Also the nominal first ML shows a slight out-of-plane slope of $M(H)$ which can be attributed to the second layer. The same twofold spin-reorientation transition was reported for Co/Ru(0001) (Refs. 46 and 59) where the magnetization reversal from in plane for 1 ML to out of plane for 2 MLs was attributed to a horizontal structural relaxation leading to an increase in the band contribution to the MAE out balancing the dipolar term, whereas for 3 ML the dipolar term dominates again favoring an in-plane orientation of the magnetization. Note that Rh(111) and Ru(0001) have almost the same in-plane lattice constant. However, the STM images for 1 ML Co/Rh(111) show that partial dislocations exist already in the monolayer limit, in variance with the argument presented in Ref. 46.

VI. THEORY

A. Computational setup

Ab initio calculations of the spin and orbital moments and of the MAE of free-standing close-packed monolayers of Fe and Co and of ultrathin films deposited on Rh and Pt(111) surfaces were carried out within DFT, using the Vienna *ab initio* simulation package (VASP).[60,61] VASP performs an iterative solution of the Kohn-Sham equations using a plane-wave basis set and describing the electron-ion interaction within the projector-augmented-wave formalism,[62,63] which allows to achieve full basis-set convergence with a reasonable computational effort. The plane-wave basis set used here contained components with energies up to 260 eV. To describe electronic exchange and correlation we employed the functional proposed by Perdew and Wang (PW91) (Ref. 64) within the generalized-gradient approximation (GGA), together with the spin interpolation according to Vosko *et al.*,[65] which is known to give reasonably accurate results both for structural and magnetic properties. Test calculations with the functional of Perdew, Burke, and Ernzerhof[66] produced almost identical results. The use of a gradient-corrected functional is especially important for Fe. Within the local-density approximation (LDA), bulk Fe is predicted to be hexagonal close packed and nonmagnetic while with the GGA the correct ground state (body-centered cubic and ferromagnetic) is found.[67] SOC is implemented in VASP in a noncollinear mode[68–70] which allows a self-consistent calculation of orbital moments and magnetic anisotropy energy. More detailed information on calculations of the MAE using VASP, as well as an assessment of the influence of different approximations can be found in Ref. 21.

For simulating the surfaces, a standard slab configuration with an in-plane (1×1) periodicity was used. Periodically repeated supercells were separated by a sufficiently large interslab vacuum layer of about 12 Å. Particular attention was given to the convergence of the calculations with respect to the slab thickness, see next section. The positions of the atoms in the adlayer and in the four topmost substrate layers of the slab were optimized using scalar relativistic calculations and a quasi-Newton algorithm based on the exact Hellmann-Feynman forces, with a force criterion for stopping the structural optimization of 0.01 eV/Å.

For each system, the geometry and electronic ground state resulting from the scalar relativistic calculation were used to

TABLE I. Calculated structural properties of the clean surfaces modeled as 11-layer slabs: Δ_{i-j} represents the distance (in Å) separating the layers i and j, the layer $i=1$ being the top uppermost atomic layer. The percentage indicated in parentheses is the relative relaxation with respect to the bulk interlayer distance of the (111) substrate defined by $d_{111}=a_0/\sqrt{3}$, wherein a_0 is the calculated bulk lattice constant; for Δ_{1-2}, relative relaxations measured experimentally are also given for comparison. An asterisk (*) indicates that the interlayer distance corresponds to the bulk interlayer distance d_{111} of the (111) substrate.

	Clean Rh(111)	Clean Pt(111)
Δ_{1-2}	2.180 (−1.8%)	2.330 (1.4%)
Expt.	(−1 ± 0.9 %, Ref. 73)	(1.3 ± 0.5 %, Ref. 74)
Δ_{2-3}	2.208 (−0.5%)	2.294 (−0.2%)
Δ_{3-4}	2.231 (0.5%)	2.295 (−0.2%)
Δ_{4-5}	2.227 (0.4%)	2.304 (0.2%)
Δ_{5-6}	2.219*	2.298*

initialize two sets of self-consistent relativistic calculations including spin-orbit coupling, for magnetic moments being oriented perpendicular and parallel to the surface. Our computational setup allows, in principle, for a noncollinear orientation of spin and orbital moments, but we always found a collinear alignment. The comparison of the calculated total energies then enables to find the easy and hard magnetic axes and to determine the electronic contribution to the MAE in terms of the difference in the total energies. Due to the small magnitude of the MAE, a very high level of convergence of the total energy is essential. Hence the self-consistency cycle was stopped only after a convergence within 10^{-7} eV has been achieved. In addition, an accurate determination of the MAE requires to use a very fine k-point mesh for the Brillouin-zone (BZ) integrations. We used Monkhorst-Pack k-point meshes[72] adapted to the size of the computational cell, as detailed below. To speed up convergence, a modest Gaussian smearing of the eigenstates with a small width of 0.01 eV was used; however, all converged total energies were extrapolated to zero smearing.

This approach based on fully self-consistent relativistic calculations for both perpendicular and parallel (in-plane) orientations of the magnetization differs from the commonly used method based on the magnetic force theorem (the MAE is calculated in terms of the difference in the band energies calculated at a frozen potential). The force theorem allows to reduce the computational effort but can also lead to errors which are difficult to control. Here we have used the force theorem to separate for the supported monolayers the contributions to the MAE coming from the magnetic adlayer and from the induced magnetization in the top layers of the substrate. The force theorem has also been used to estimate the contribution of orbitals of different symmetry to the MAE. However, within our plane-wave approach, the calculation of angular momentum and layer-decomposed densities of states (DOSs) requires the projection of the plane-wave components of the eigenstates onto spherical waves within atomic spheres. The radius of these spheres has been chosen such that its volume is equal to the atomic volume, leading to slightly overlapping spheres. It must be kept in mind that this procedure is necessarily approximate so that it cannot be expected that the sum of the layer- and/or angular momentum decomposed contributions to the MAE matches exactly that calculated from the total density of states. In addition to the electronic or band contribution, the MAE depends also on the dipolar interactions between the magnetic moments. The dipolar contribution is non-negligible already in the monolayer limit and increases with increasing film thickness. A detailed comparative study of the impact of such approximations on calculations of the MAE has recently been published for Fe and Co adatoms on a Pt(111) surface.[21]

B. Bulk metals and clean surfaces

For assessing the reliability of our computational setup, we first present the results obtained for the bulk metals and clean surfaces considered in this study. These results will also serve later as basis for analyzing the properties of the adlayer covered substrates.

Using a sufficiently dense Monkhorst-Pack grid of $12\times12\times12$ for the primitive cubic cell of fcc Rh, fcc Pt, hcp Co, and bcc Fe, the lattice constants are found to be in good agreement with the experimental values given in brackets:[75,76] $a_0^{\mathrm{Rh}}=3.843(3.803)$ Å, $a_0^{\mathrm{Pt}}=3.980(3.924)$ Å, $a_0^{\mathrm{Co}}=2.493(2.507)$ Å, $c_0^{\mathrm{Co}}=4.016(4.069)$ Å, and $a_0^{\mathrm{Fe}}=2.801$ (2.867) Å. On the other hand, too small lattice constants, e.g., 3.765 Å for Rh, are found within the LDA. Because of the different crystal structures of the bulk metals, the size mismatch should be calculated from the equilibrium atomic volumes, $V_0=15.76(15.08)/14.19(13.76)/12.47(12.79)/10.99(11.78)$ Å^3 for Pt/Rh/Co/Fe, respectively (experimental atomic volumes in parentheses). The linear size mismatch derived from these volumes varies between 0.886(0.921) for Fe/Pt and 0.958(0.976) Co/Rh, the experimental values are again given in parentheses. Hence one should keep in mind that the GGA calculations tend to overestimate the stress and strain in the film imposed by the epitaxial constraint. But it must also be emphasized that to use the experimental lattice constant of the substrate is not a solution, in this case both the film and the substrate would be under considerable stress.

The spin magnetic moments obtained for the magnetic metals from scalar relativistic calculations based on the GGA are also in very good agreement with the experimental estimations: $\mu_0^{\mathrm{Co}}=1.581(1.58)\ \mu_B$ and $\mu_0^{\mathrm{Fe}}=2.152(2.22)\ \mu_B$, whereas the LDA similarly leads to substantially underestimated spin magnetic moments, such as 1.479 μ_B for Co. In the following, results are given using the GGA only.

As already investigated theoretically,[36] a minimum slab thickness is necessary to accurately describe the magnetic properties of clean Rh(111) and Pt(111) surfaces. Indeed, spin-polarized calculations for too thin Rh slabs lead to weakly magnetic slabs, using both the LDA or the GGA. A thickness on the order of eight layers or more appears to be sufficient for correctly describing the absence of surface magnetism on the (111) surfaces of bulk Rh and Pd. It should, however, be emphasized that the formation of a weak magnetic moment on the surfaces of very thin layers is not a spurious effect. The investigations of Shinohara *et al.*[32] on

TABLE II. Calculated magnetic properties of free-standing hexagonally close-packed Co and Fe monolayers with interatomic distances $d_{\text{M-M}}$ corresponding either to the relaxed geometry ($d_{\text{Co-Co}}$=2.343 Å, $d_{\text{Fe-Fe}}$=2.396 Å) or to an expanded geometry matching the surface of the Rh(111) substrate ($d_{\text{M-M}}$=2.717 Å) or Pt(111) substrate ($d_{\text{M-M}}$=2.814 Å). Spin and orbital moments μ_S and μ_L are given in units of μ_B/atom, as resulting from a scalar calculation or from relativistic calculations including SOC assuming an out-of-plane ($\perp$) or an in-plane ($\parallel$) orientation of the magnetic moments. $E_a(electr.)$ and $E_a(dipole)$ represent the band and dipolar contributions to the total MAE E_a; all MAE values are given in meV/adatom (a negative value indicates an in-plane easy axis). Numbers in parentheses give the MAE as calculated using the magnetic force theorem and the frozen potential derived from calculations from perpendicular magnetization, cf. text.

	Free-standing hexagonally close-packed Fe ML								
	Relaxed			Matching Rh(111)			Matching Pt(111)		
Magnetic moments	scalar	$\perp$	$\parallel$	scalar	$\perp$	$\parallel$	scalar	$\perp$	$\parallel$
μ_S	2.526	2.539	2.546	3.006	3.000	3.000	3.066	3.059	3.060
μ_L		0.092	0.060		0.097	0.089		0.111	0.096
Magnetic anisotropy									
$E_a(electr.)$	1.10(1.19)				0.50(0.90)			0.60(0.58)	
$E_a(dipole)$	−0.4				−0.4			−0.4	
$E_a=E_a(electr.)+E_a(dipole)$	0.7				0.1			0.2	
Easy axis	$\perp$				$\perp$			$\perp$	
	Free-standing hexagonally close-packed Co ML								
	Relaxed			Matching Rh(111)			Matching Pt(111)		
Magnetic moments	Scalar	$\perp$	$\parallel$	Scalar	$\perp$	$\parallel$	Scalar	$\perp$	$\parallel$
μ_S	1.822	1.815	1.818	2.058	2.060	2.057	2.084	2.078	2.079
μ_L		0.064	0.140		0.155	0.262		0.184	0.313
Magnetic anisotropy									
$E_a(electr.)$		−0.29(−0.41)			−1.22(−1.20)			−1.65(−1.56)	
$E_a(dipole)$		−0.25			−0.22			−0.21	
$E_a=E_a(electr.)+E_a(dipole)$		−0.54			−1.44			−1.86	
Easy axis		$\parallel$			$\parallel$			$\parallel$	

fine Pd particles with radii around 100 Å have confirmed the ferromagnetic character of their surfaces while no surface magnetism is found on bulk samples. The calculations for surfaces covered by a magnetic adlayer described in the next sections have been performed on slabs consisting of at least 11 layers. In this case the long-range magnetic polarization of the substrate induced by the magnetic adlayer is slightly enhanced by surface effects at the bottom of the slab.[36] This creates a slight difference compared with the experiments performed on thick substrates. An 11-layer slab turned out to be a reasonable compromise between the computational cost and the accurate description of the Rh or Pt(111) substrates.

The results are presented in Table I. In good agreement with the experiments,[73,74] the clean Rh(111) surface is found to exhibit a modest inward relaxation of the top uppermost layer by −1.8%, whereas on the other hand, in the clean Pt(111) surface the top layer is modestly relaxed outward by 1.4%. The relaxation of the deeper layers is much less significant and remains inferior to 0.5% and 0.2% in Rh and Pt surfaces, respectively.

C. Free-standing Co and Fe ultrathin films

Before turning to magnetic monolayers supported on nonmagnetic Rh(111) and Pt(111) substrates we analyze the properties of free-standing hexagonally close-packed Co and Fe monolayers. Both monolayers with interatomic distances relaxed to their equilibrium values ($d_{\text{Co-Co}}$=2.343 Å, $d_{\text{Fe-Fe}}$=2.396 Å) and constrained to match the Rh(111) ($d_{\text{M-M}}$=2.717 Å) and Pt(111) ($d_{\text{M-M}}$=2.814 Å) substrates have been considered. This will help to assess the effect of the reduced dimensionality, of the intralayer strain imposed by the epitaxial growth, and of the hybridization of the eigenstates of adlayer and substrate atoms at the interface, and their consequences on the magnetic properties of the decorated surfaces.

The results obtained using a 1×1 surface cell and a two-dimensional $28\times28\times1$ k-point mesh are summarized in Table II. Even if the results, in particular, the calculated MAE, are in most cases almost identical to those obtained for a k-point mesh of $12\times12\times1$ only, Fig. 6 shows that for a strained Co(111) ML such a very dense k-point sampling is necessary to achieve absolute convergence of the band contribution to the MAE within 0.1 meV/Co atom.

As expected, the spin moments obtained from the scalar spin-polarized calculations are strongly enhanced with respect to bulk Co and Fe as a consequence of the reduced coordination in the film and the resulting narrowing of the d-band width. As in the bulk metals, the spin moment of the Fe atoms is found to be larger than for Co. If the in-plane

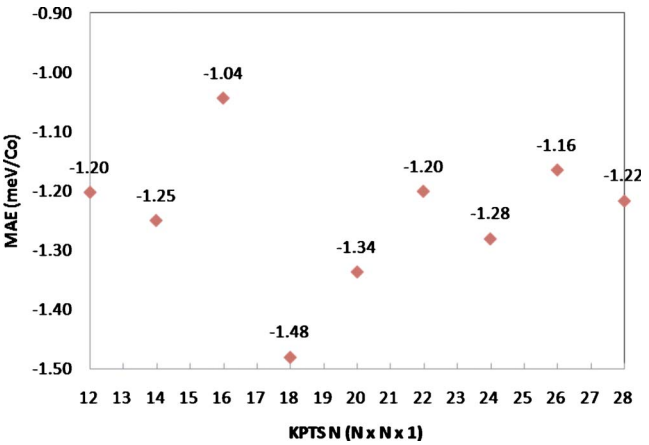

FIG. 6. (Color online) Convergence of the band contribution to the MAE of a free-standing Co(111) ML expanded to match the Rh(111) substrate with respect to the density of the Brillouin-zone sampling.

lattice constant within the monolayers is further expanded to match that of the Rh or Pt substrates (which corresponds to lattice constant expansions of about 16–20 % and 13–17 % for Co and Fe, respectively, which is much larger than the bulk lattice misfit since the free-standing layers have significantly smaller in-plane lattice constants), we find a further enhancement resulting from a further band narrowing.

If SOC is taken into account, the spin moments remain almost unchanged. Orbital moments remain small in comparison; they are larger in the Co ML than in the Fe ML, in contrast to the trend observed for the spin moments. The orbital moments also generally increase with the increase in the interatomic distances, in line with the reduced interatomic hybridization. While the spin moments are almost isotropic, the orbital moments are anisotropic. The orbital anisotropy is weak in the Fe ML ($\Delta\mu_L \sim 0.01-0.03\ \mu_B$, a positive sign stands for a larger perpendicular moment) but quite important for a Co ML ($\Delta\mu_L \sim -0.08$ to $-0.13\ \mu_B$, increasing with the interatomic distance).

For the Fe ML constrained to match the Rh or Pt substrates we calculate an electronic contribution to the MAE of $E_a(electr.)=0.5-0.6$ meV/atom (the positive sign of the MAE always indicates perpendicular anisotropy) while for a relaxed Fe ML we find a larger value of $E_a(electr.)=1.1$ meV/atom. Calculations for the constrained MLs using the magnetic force theorem and a frozen potential from converged out-of-plane calculations yield to semiquantitative agreement with the total-energy calculations. In contrast, for a relaxed Co ML we calculate a modest negative MAE of $E_a(electr.)=-0.29$ meV/atom, increasing to more negative values of $E_a(electr.)=-1.22(-1.65)$ meV for MLs constrained to match Rh(111) [Pt(111)]. Again we find using the force theorem a reasonable agreement with the more accurate results from the total-energy differences. Despite the lower accuracy, the force theorem proved to be very helpful in analyzing the electronic origin of the MAE, because it allows a decomposition into contributions from different orbitals.

To obtain the total MAE, the dipolar energy has to be added. The dipolar term always favors in-plane magnetization. For a Fe ML, this leads to a reduction in the positive MAE to 0.7 meV/atom for a relaxed ML and to 0.1 (0.2) meV/atom for MLs matching the Rh (Pt) substrate, depending on the constraint, this is close to the limit of the precision of the calculation. For the Co ML, the dipolar term enhances the preference for in-plane magnetization, yielding total MAEs of $E_a=-0.54$ meV/atom, -1.4 meV/atom, and -1.86 meV/atom for relaxed, Rh, and Pt in-plane lattice constants, respectively. For both free-standing Fe and Co MLs, the magnitude of the MAE is found to increase with increasing tensile strain, this correlates with the increase in the orbital moments with increased interatomic distances.

Bruno[77] has developed a perturbation theory for the electronic contribution to the magnetic anisotropy predicting that the MAE is proportional to the product of the strength ζ of the SOC times the anisotropy $\Delta\mu_L=\mu_L^{\perp}-\mu_L^{\parallel}$ of the orbital moments, i.e., $E_a(electr.)\propto\zeta\times\Delta\mu_L$. For both Co and Fe MLs the sign of MAE and orbital anisotropy are the same as expected from Bruno's theory, and the stronger magnetic anisotropy of the Co ML also corresponds to its larger orbital anisotropy.

An early calculation of the MAE of free-standing Co(111) monolayers using the linear muffin-tin orbital method in the atomic-sphere approximation, the local-density approximation, and the magnetic force theorem was reported by Daalderop *et al.*[78] The MAE was calculated as a function of the band filling. For a realistic value of the band filling between 9.0 and 9.4 electrons a negative (in-plane) MAE of 1.0–3.5 meV/atom was reported. Given the differences in the choice of the basis set, exchange-correlation potential, and approach to the MAE, their value is in surprisingly good agreement with our results. Daalderop *et al.* also explored the electronic origin of the MAE. We slightly extended their line of arguments below to analyze our results and to put them in perspective with the MAE calculated for other nanostructures.

Electronic origin of the MAE

According to Daalderop *et al.*[78] two distinctly different contributions to the MAE can be distinguished: (i) the splitting of partially occupied degenerate eigenstates by the SOC results in a lowering of the total energy. The existence of twofold degenerate d states in magnetic nanostructures depends on their symmetry. In a scalar relativistic approach the Hamiltonian commutes with L_z, the projection of the orbital angular momentum operator onto the axis of a dimer or a monatomic wire or onto a direction perpendicular to the surface of a monolayer. The electronic eigenstates can hence be labeled according to the eigenvalues $m=0,\pm1,\pm2$ (in units of $\hbar$) of L_z, corresponding to the one- ($m=0$) and two-dimensional ($m=\pm1,\pm2$) representations of the group $C_{\infty v}$ (for a dimer or wire) or of the group C_h for a monolayer. Bands with $\pm m$ are degenerate due to the mirror symmetry with respect to the plane of the ML or a plane containing the axis. In the nonmagnetic case, states are further degenerate with respect to the spin. If SOC is taken into account, spin and orbital degrees of freedom are coupled and eigenstates are labeled by the half-integer eigenvalues $m_j=\pm1/2,\pm3/2,\pm5/2$ of the operator of the z component of the total angular momentum $J_z=L_z+S_z$. In the nonmagnetic

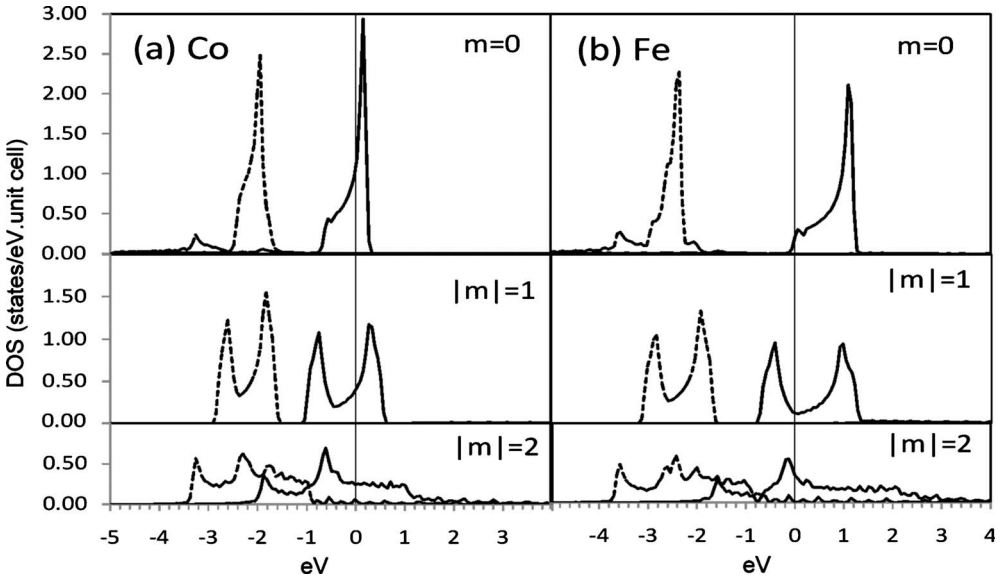

FIG. 7. Majority-spin (dashed lines) and minority-spin (solid lines) orbital-projected *d*-electron density of states for free-standing hexagonally close-packed (a) Co and (b) Fe monolayers.

case mirror-symmetry and time-reversal symmetry in combination with inversion symmetry are preserved, and bands with $\pm m_j$ are degenerate. This twofold degeneracy is broken when the wire is magnetized along the axis since reflection and time reversal are no longer symmetry operations. The symmetry is reduced from $C_{\infty v}$ to C_∞ with one-dimensional irreducible representations only. The magnetization is an axial vector and hence reverses its direction under both time reversal and mirror symmetry but not under inversion. For perpendicular (transverse) magnetization reflection symmetry with respect to a plane containing the dimer (wire) axis and perpendicular to the magnetization direction is preserved, the symmetry double group is C_s^D. There are three twofold degenerate states, one with $m_j = \pm 5/2$ and two with $m_j = \pm 1/2$. If one or more of these states are located close to the Fermi level, the splitting induced by parallel magnetization results in a lowering of the total energy. It has been demonstrated that the lifting of twofold degeneracies determines the parallel magnetic anisotropy of certain transition-metal dimers (such as, e.g., Co_2) (Refs. 79 and 80) and of Pt nanowires.[81,82] In monolayers, twofold degeneracies related to the mirror symmetry with respect to the plane of the monolayer can occur only at high-symmetry points of the two-dimensional Brillouin zone, at the Γ and K points for triangular (111) planes. In-plane magnetization preserves the mirror symmetry but it is lifted for perpendicular magnetization. If these degeneracies occur at the Fermi energy, their splitting gives a contribution to the MAE favoring perpendicular magnetization.

(ii) A further contribution to the MAE comes from the coupling of eigenstates with energies above and below the Fermi energy through the spin-orbit interaction. Within a perturbative treatment (which is justified if the level splitting $\Delta_{ij} = E_i - E_j$ is larger than the spin-orbit coupling parameter), the contribution to the MAE from each pair of states is given by

$$\Delta E_{ij} = \frac{1}{\Delta_{ij}}[|H^{SO}(\vec{x})|^2 - |H^{SO}(\vec{z})|^2], \tag{3}$$

where $H^{SO}(\vec{n}) = \langle \psi_i | H^{SO}(\vec{n}) | \psi_j \rangle$ is the matrix element of the spin-orbit coupling operator between states ψ_i and ψ_j with eigenvalues E_i and E_j. For a magnetization direction along $\vec{n}$ the spin-orbit interaction matrix has the form

$$H^{SO}(\vec{n}) = \zeta/2 \begin{pmatrix} \vec{n}\cdot\vec{L} & \vec{n}_\perp \cdot \vec{L} + \frac{1}{2}\Delta L \\ \vec{n}_\perp \cdot \vec{L} + \frac{1}{2}\Delta L & -\vec{n}\cdot\vec{L} \end{pmatrix}, \tag{4}$$

where ζ is the spin-orbit coupling parameter and $\Delta L = (L_- - L_+)$. This contribution can favor either perpendicular or in-plane magnetization, depending on the spins and symmetries of the interacting states. According to the detailed analysis presented by Daalderop *et al.*,[78] in-plane magnetization (i.e., parallel to $\vec{x}$) is favored if the Fermi energy is located between even ($m = 0, \pm 2$) and odd ($m = \pm 1$) states of the same spin, or between even (or odd) states of opposite spin because the coupling $\frac{\zeta}{2}\vec{n}\cdot\vec{L}$ is nonzero only for $\vec{n} = \vec{x}$. In contrast, the coupling between even states of one spin and odd states of opposite spin is nonzero only if $\vec{n} = \vec{z}$. Hence perpendicular anisotropy is favored if the Fermi level is located between odd ↑ and even ↓ states or between even ↑ and odd ↓ states (although the former contribution is strongly reduced by a large energy denominator Δ_{ij}).

The preceding analysis prepares a discussion of the origin of the different sign of the MAE in free-standing Co(111) and Fe(111) monolayers. The spin-polarized orbital-projected *d*-electron densities of states for both monolayers are shown in Fig. 7, they differ considerably because of the different directionality of the orbitals. The $m = 0$ DOS is very narrow and exhibits a sharp peak at the upper edge arising from a nearly dispersionless band along the BZ boundary.

The $|m|=1$ DOS shows two peaks close to the upper and lower edges, the bonding states are located predominantly at the K point, the antibonding states at the Γ point. The $|m|=2$ DOS is rather broad with less pronounced Van Hove singularities at the bottom and near the center of the band. The Van Hove peaks in the $m=\pm 1, \pm 2$ DOS arise from the double-degenerate stationary states at the high-symmetry points. The Co and Fe DOSs differ mainly by the width of the exchange splitting (on average $\Delta_{xc} \sim 2$ eV for Co, $\Delta_{xc} \sim 3$ eV for Fe, the splitting is largest for the $m=0$ and smallest for the $m=\pm 2$ states) and by the band filling. For both Co and Fe MLs all majority bands are completely occupied. For Co the $m=0$ minority band is about half filled, whereas for Fe it is empty. The Fermi energy is located just above (Co) or below (Fe) the minimum in the partial $m=\pm 1$ minority DOS, for Fe the peak in the $m=\pm 2$ minority DOS is located very close to the Fermi level, whereas it is shifted to greater binding energies for Co.

For Co the splitting of the degenerate eigenstates plays no significant role because these states are far enough from the Fermi edge. A spin-orbit-mediated coupling between occupied and empty states is possible between the empty antibonding $m=0$ (even) and the occupied bonding $|m|=1$ (odd) down-spin states and between empty antibonding $|m|=1$ (odd) and the occupied $m=\pm 2$ down-spin states just below E_F, both favor in-plane magnetization. The contributions from other interactions involving even and odd states of opposite spins is reduced by a large energy denominator. However, this analysis of the spin-orbit-mediated coupling between eigenstates provides just a qualitative hint to the mechanisms governing the sign and magnitude of the MAE. A quantitatively more reliable, although still approximate analysis is possible using the angular momentum decomposed partial DOS and the force theorem. In this approximation, the MAE may be written as

$$E_a = \sum_i \sum_{m=-2}^{m=2} \int_{E_B}^{E_F} (E - E_F) \Delta n_m^i(E) dE, \tag{5}$$

where the sum is over all atoms i in the supercell and over all angular momentum quantum numbers m, and where

$$\Delta n_m^i(E) = n_m^i(E;\perp) - n_m^i(E;\parallel) \tag{6}$$

is the difference in the partial local densities of states for electrons with quantum number m at the site i for perpendicular and in-plane (parallel) magnetization. Integration over the $\Delta n_m^i(E)$ also yields the orbital anisotropy $\Delta\mu_L = \mu_L^{\perp} - \mu_L^{\parallel}$ according to

$$\Delta\mu_L = 2\mu_B \sum_i \sum_{m=1,2} \int_{E_B}^{E_F} [\Delta n_m^i(E) - \Delta n_{-m}^i(E)] dE. \tag{7}$$

The analysis of the orbital-decomposed DOS shows immediately that for the Co ML the by far dominant contribution to the orbital anisotropy comes from the out-of-plane states with $m=\pm 1$ while the in-plane orbitals with $m=\pm 2$ are almost independent of the orientation of magnetization. This is demonstrated in Fig. 8(a) which shows the $\Delta n_m(E)$ (orbital-decomposed DOS integrated over all sites), together

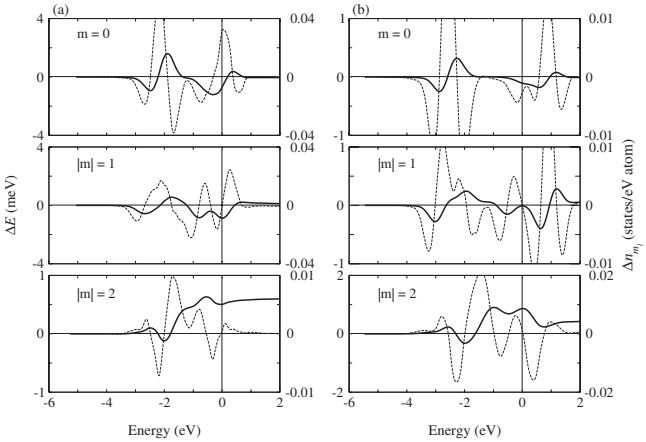

FIG. 8. Changes $\Delta n_m(E)$ in the angular momentum decomposed density of states with reorientation of the magnetization direction (dashed lines and left-hand scales) and integrated angular momentum decomposed contributions to the MAE (bold lines are right-hand scales) for $|m|=0,1,2$ in free-standing (a) Co and (b) Fe MLs strained to match the Rh(111) in-plane lattice constant, cf. text.

with the angular momentum decomposed contributions to the MAE of a free-standing Co ML strained to match the Rh(111) surface, calculated as a function of the band filling. The diagram shows that the dominant contributions come from binding energies up to about −1.5 meV below E_F, spin-orbit-induced differences in the DOS at larger binding energies largely cancel. The negative MAE arises, as expected from the arguments discussed above, from the $m=0$ (−0.77 meV/atom) and the $m=\pm 1$ (−0.89 meV/atom) states, while the contribution from the $m=\pm 2$ states is positive (0.53 meV/atom). The sum of these values is −1.13 meV/atom, in very good agreement with the total MAE of −1.22 meV/atom calculated from the total-energy (TE) difference or −1.20 meV/atom from the force theorem (FT) and the total DOS. Perfect agreement is not to be expected since the calculation of the partial DOS is based on a projection of the plane-wave components of the eigenstates onto spherical waves within atomic spheres. The same analysis for a Co ML strained to match a Pt(111) surface leads to an analogous result with a dominant negative contribution from $m=0, \pm 1$ (−0.11 meV/atom and −1.37 meV/atom, respectively) and a positive contribution (0.47 meV/atom) from $m=\pm 2$ states, together −1.01 meV/atom to be compared with an MAE of −1.56 meV/atom (FT) or −1.65 meV/atom (TE). It is interesting that although the orbital anisotropy arises only from $m=\pm 1$ states, all orbitals contribute to the MAE. This reflects the importance of off-diagonal contributions as discussed above.

For the Fe ML the orbital anisotropy is dominated by the $m=\pm 1$ and $m=\pm 2$ orbitals. For a Fe(111) ML the minority states are shifted farther above the Fermi level, leading to a reduction in the interactions favoring in-plane anisotropy for Co because of a larger energy denominator. The MAE is now dominated by the splitting of the degenerate $m=\pm 2$ down-spin states close the E_F, favoring perpendicular anisotropy. Again this is confirmed by an analysis of the angular momentum decomposed contributions via the force theorem, see Fig. 8(b). In this case we calculated a dominant positive

TABLE III. Calculated structural and energetic properties of the most stable pseudomorphic adlayer-substrate systems (same notations as in Table I). The adsorption energy E_{ads} is given in eV/adatom (a negative value indicates an exothermic process). Since the granular films in experiment imply both adsorption sites results are also presented for the metastable hcp Fe/Pt(111) system (see text).

	hcp Co/Rh(111)	hcp Co_2/Rh(111)	hcp Fe/Rh(111)
E_{ads}	−1.77	−1.83	−1.58
Δ_{1-2}	1.995 (−10.1%)	1.815 (−18.2%)	2.057 (−7.3%)
Δ_{2-3}	2.244 (1.1%)	2.073 (−6.6%)	2.242 (1.0%)
Δ_{3-4}	2.218 (−0.1%)	2.239 (0.9%)	2.216 (−0.1%)
Δ_{4-5}	2.219 (0.0%)	2.210 (−0.4%)	2.217 (−0.1%)
Δ_{5-6}	2.219*	2.224 (0.2%)	2.219*
	hcp Co/Pt(111)	fcc Fe/Pt(111)	hcp Fe/Pt(111)
E_{ads}	−1.81	−1.84	−1.82
Δ_{1-2}	1.996 (−13.2%)	2.039 (−11.3%)	2.044 (−11.1%)
Δ_{2-3}	2.365 (2.9%)	2.385 (3.8%)	2.382 (3.7%)
Δ_{3-4}	2.322 (1.1%)	2.323 (1.1%)	2.321 (1.0%)
Δ_{4-5}	2.310 (0.5%)	2.307 (0.4%)	2.309 (0.5%)
Δ_{5-6}	2.298*	2.298*	2.298*

contribution from the $m=\pm 2$ states (0.80 meV/atom). A much smaller negative contribution (−0.10 meV/atom) comes from $m=0$ states and an almost vanishing contribution (−0.01 meV/atom) from $m=\pm 1$ (although these orbital determine the orbital anisotropy), together 0.69 meV/atom, in comparison the total MAE is 0.90 meV/atom (FT) and 0.50 meV/atom (TE). For a Fe ML matching the Pt(111) surface we calculate contributions of −0.17, −0.03, and 2.13 meV/atom for $m=0, \pm 1, \pm 2$, together 1.93 meV/atom to be compared to a total MAE of 0.58 meV/atom (FT) or 0.60 meV/atom (TE). In this case the angular momentum decomposition introduces a larger error but this does not affect the conclusion concerning the mechanism determining the sign of the MAE.

D. Co and Fe ultrathin films on Rh and Pt substrates

1. Energetics and structure

Table III summarizes the structural and energetic properties of Co and Fe monolayers deposited on the Rh and Pt(111) surfaces as calculated in a spin-polarized scalar-relativistic approach. As previously mentioned, the Rh(111) and Pt(111) surfaces are modeled by 11-layer slabs. Both fcc and hcp stacking of the Fe/Co adlayer on the surfaces of the fcc crystals have been considered. For the Rh(111) surface, hcp stacking is preferred for both Fe and Co films by a modest energy difference 11 meV/Fe and 5 meV/Co, respectively. On the Pt(111) surface, Co adatoms also prefer to occupy a hcp hollow whereas Fe atoms show a more marked preference for the fcc hollows (energy difference of 21 meV/Fe). The same preference for hcp adsorption sites has also been found for isolated Co and Fe atoms on these substrates,[21,71] but with much higher energy difference [for Fe(Co) adatoms on Rh(111) the hcp adsorption site is 89(88) meV/atom lower in energy]. Even more important is the result that the barrier for hopping diffusion between the two different hollows is even larger, 198(219) meV for Fe(Co) on Rh(111). This means that atoms deposited at low temperatures will stick to their initial adsorption sites and granular films with lower than monolayer coverage will consist of regions with fcc and hcp stacking.

The adlayers strongly relax inward by 7% [Fe/Rh(111)] to 13% [Co/Pt(111)] of the ideal interlayer distances of the substrates. The stronger relaxation on the Pt substrate is expected due to the larger lattice constant of Pt. The inward displacement is slightly larger than expected from the size mismatch alone, indicating a strong adsorbate/substrate binding. The interlayer distances within the substrates are hardly affected beyond the four topmost Rh or Pt layers, only the top layer of the substrate undergoes an outward relaxation ranging between 1% [Co/Rh(111)] and 3.8% [Fe/Pt(111)]. The adsorption energy E_{ads} is defined as the energy gained or released during pseudomorphic adsorption of a Fe or Co monolayer constrained to match the substrate. With this definition E_{ads} accounts only for the strength of the chemical interaction between adlayer and substrate and is therefore a good indicator of the hybridization of adsorbate and substrate orbitals at the interface. E_{ads} is always negative (exothermic), ranging between −1.6 and −1.8 eV/adatom, indicating a strong adlayer-substrate hybridization and explaining the strong inward relaxation.

For Co/Rh(111), we determined also the geometry and adsorption energy of a Co bilayer. A hcp stacking is found to be preferred. The distance between the two Co layers is strongly contracted while the distance between the Co and Rh layers is slightly larger than for the monolayer. The binding energies for monolayer and bilayer allow to estimate an eventual preference for island formation during the film growth. From the total energies of 1 ML and 2 ML Co films adsorbed on the Rh substrate we can determine a possible tendency to island formation if we assume that islands formed at the surface are sufficiently large so that contributions of edge and side facets to the total energy are negligible. Under this assumption, the energy change per surface unit ΔE resulting from the decomposition of a smooth 1-ML-thick Co film into a clean substrate partially covered by 2 ML high islands is given by

$$\Delta E = (E_0 + E_2)/2 - E_1, \tag{8}$$

where E_n is the total energy of a compact n-ML-thick Co film adsorbed on Rh(111). With this definition, a negative value of ΔE expresses favorable conditions for island formation. From the calculated total energies we derive a value of $\Delta E = -157$ meV/Co atom, i.e., island formation is found to be energetically favored, in agreement with the experimental findings for Co/Pt(111).[87]

2. Magnetic moments

As expected from previous studies of nonmagnetic surfaces covered by magnetic adlayers,[36] Fe and Co monolayers

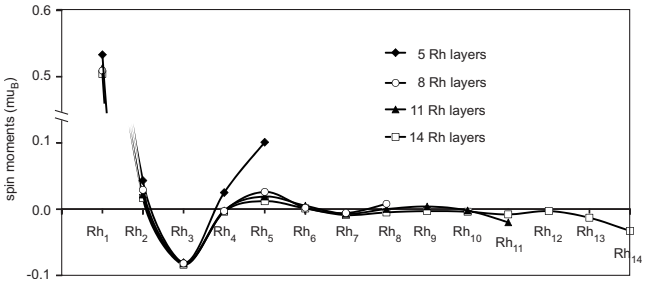

FIG. 9. Spin moments induced in the Rh(111) substrate by a Co adlayer as a function of the slab thickness.

induce significant magnetic moments in the Rh and Pt substrates. Figure 9 illustrates the profile of the induced magnetization in a Rh(111) substrate covered by a Co adlayer, as determined by calculations for slabs of increasing thickness. The topmost Rh substrate layer, which is in direct contact to the magnetic adlayer has the largest induced spin moment of about 0.5 μ_B, i.e., approximately 25% of the Co spin moment. In the deeper Rh layers we find long-range oscillatory decaying magnetic moments, as already demonstrated in our previous work.[36] Antiferromagnetic moments are induced at intermediate distances from the Co adlayer. As a consequence, somewhat surprisingly, the effective magnetic moment of the Co atom $\mu_{eff}^{\mathrm{Co+Rh}}$, defined as the sum of the Co moment and of the induced polarization of the host atoms even decreases when the slab thickness is increased: integrating the Rh moments over the whole slab, we find 2.59 μ_B, 2.45 μ_B, 2.41 μ_B, and 2.33 μ_B for Rh slabs of 5, 8, 11, and 14 layers, respectively.

However, due to the reduced coordination at the surface the magnetic moments induced at the bottom of the slabs are slightly enhanced. As discussed above, this enhancement is not necessarily unphysical, it merely reflects the limited thickness of the slab. However, it is a spurious effect if we use the slab as a model for the surface of the nonmagnetic bulk. This effect appears even for the thickest slabs which are entirely nonmagnetic in the absence of a magnetic overlayer. The conclusion is that a compromise should be found to get magnetic properties sufficiently close to convergence with respect to the slab thickness while keeping the computational effort tractable. If in the calculation of the total effective moment per Co atom, $\mu_{eff}^{\mathrm{Co+Rh}}$, one disregards the three layers at the bottom, i.e., the layers after a node in the oscillatory decaying moments, we find $\mu_{eff}^{\mathrm{Co+Rh}}$ equal to 2.55 μ_B, 2.45 μ_B, 2.43 μ_B, and 2.38 μ_B for Rh slabs of 5, 8, 11, and 14 layers, respectively. These considerations show that a 11-layer-thick slab seems to be sufficient to get $\mu_{eff}^{\mathrm{Co+Rh}}$ converged within 0.1 μ_B, provided the spurious magnetic moments induced at the bottom layers of the slab are not taken into account. Our test calculations of the MAE in these systems furthermore show that such a slab also allows to determine the MAE within 0.1 meV/Co atom, as described in the next section. Therefore, the results presented hereafter, in particular, in Table IV, have been obtained with this configuration.

Table IV summarizes the magnetic properties of Co(Fe)/Rh(111) and Co(Fe)/Pt(111) films, calculated using a slab with 11 substrate layers and a Monkhorst-Pack k-point mesh of $12\times12\times1$. Calculations have been performed both in a scalar relativistic mode and including SOC. Spin-orbit coupling causes only minimal changes in the spin moments of the adlayers. The spin moments induced in the top layers of the surface are reduced by a modest amount [the effect is largest on Pt(111) where the moments decrease by 0.03–0.04 μ_B], more remarkable is the faster decay of the induced moments with increasing distance from the interface. Again this effect is much larger for a Pt than for a Rh substrate. The most important results of the fully relativistic calculations can be summarized as follows: (i) SOC leaves the spin moments in the film almost unchanged but they are slightly reduced compared to the free-standing MLs. The decrease in the moments is modest on the Pt(111) substrate (about −0.06 μ_B) and much more pronounced on Rh(111) where the spin moments decrease by −0.10 μ_B and −0.18 μ_B for Co and Fe, respectively. The spin moments are almost isotropic, the largest anisotropy of $\Delta\mu_S=0.003$ μ_B is found for Fe/Pt(111).

(ii) The orbital moments of the Fe atoms in the adlayers are only slightly decreased (by at most −0.02 μ_B relative to the free-standing ML), whereas the orbital moments of the Co atoms change rather dramatically. For perpendicular magnetization the decrease is still relatively modest [by −0.031 μ_B on Rh(111) and −0.064 μ_B on Pt(111)] while they decrease for in-plane magnetization by −0.141 μ_B and −0.225 μ_B on Rh and Pt, respectively. This is a first indication of a much stronger hybridization at the interface of a Co adlayer with the substrate than for a Fe ML. As a consequence, the anisotropy of the orbital moments is strongly reduced, it even changes sign. In all cases we now find a larger orbital moment for perpendicular magnetization, it is now largest for Co/Pt(111) with $\Delta\mu_L=0.032$ μ_B (to be compared to $\Delta\mu_L=-0.129$ μ_B for a free-standing matching Co ML).

(iii) The magnetic moments induced by a Co overlayer are always much larger than those induced by a Fe layer. The difference is very large on the Rh(111) substrate where we calculate induced moments in the first substrate layer of $\mu_S(\mathrm{Rh}_1)=0.524$ μ_B and 0.158 μ_B for hcp Co and Fe MLs, respectively. On a Pt(111) substrate the difference is less pronounced with $\mu_S(\mathrm{Pt}_1)=0.362$ μ_B and 0.302 μ_B for hcp Co and Fe MLs, respectively. The induced moments depend also the adsorption site: if the Fe atoms on Pt(111) are placed into the fcc instead of the hcp hollows the induced spin moments decrease by about 0.04 μ_B. This difference can be explained in terms of the differences in the overlap of the d bands of adlayer and substrate. Due to the larger exchange splitting of the Fe d band, the overlap with the Rh d band is reduced, leading to a weaker hybridization and thus to a reduced induced moment. The nature of the adlayer also influences the oscillating profile of the induced magnetic polarization of the substrate: for hcp Fe/Rh(111) antiferromagnetic moments are indeed observed already on the second Rh layer. The d band of Pt is broader than that of Rh, hence the differences in the exchange splitting of Co and Fe do not lead to a significant difference in the d-band overlap. It is remarkable that in all cases the total effective spin moment per magnetic atom is quite modest: for a Co ML on both Rh and Pt substrates we calculate an effective spin moment of about 2.44 μ_B/Co

TABLE IV. Magnetic properties of the most stable pseudomorphic adlayer-substrate systems (same notations as in Table II), calculated for 11-layer slabs and a $(12\times12\times1)$ k-point mesh for Brillouin-zone integrations. For sake of comparison, results are also given for the metastable hcp Fe/Pt(111) system (see text). μ_S (ΣM) and μ_L (ΣM), where M=Rh and Pt, represent the total spin and orbital moments induced in the substrate (disregarding the three substrate layers, see text).

	hcp Co ML on Rh(111)			hcp Co bilayer on Rh(111)			hcp Fe ML on Rh(111)		
Magnetic moments	Scalar	⊥	∥	Scalar	⊥	∥	Scalar	⊥	∥
μ_S (Co_2)				1.829	1.823	1.824			
μ_S (Co_1/Fe)	1.966	1.964	1.965	1.795	1.791	1.791	2.820	2.824	2.822
μ_S (Rh_1)	0.531	0.524	0.524	0.258	0.255	0.257	0.161	0.158	0.154
μ_S (Rh_2)	0.028	0.020	0.024	−0.028	−0.028	−0.029	−0.105	−0.101	−0.104
μ_S (Rh_3)	−0.083	−0.087	−0.086	−0.052	−0.051	−0.049	−0.032	−0.027	−0.031
μ_S (Rh_4)	−0.003	−0.006	−0.007	−0.002	0.003	0.005	0.017	0.025	0.022
μ_S (ΣRh)	0.494	0.472	0.484	0.186	0.173	0.182	0.026	0.051	0.026
μ_L (Co_2)					0.120	0.113			
μ_L (Co_1/Fe)		0.124	0.121		0.092	0.079		0.091	
μ_L (Rh_1)		0.023	0.023		0.002	0.001		0.005	−0.003
μ_L (Rh_2)		−0.001	−0.004		−0.002	−0.006		−0.007	−0.004
μ_L (Rh_3)		−0.003	−0.004		−0.002	−0.004		0.000	0.000
μ_L (Rh_4)		0.000	0.001		0.000	0.001		0.001	0.002
μ_L (ΣRh)		0.022	0.017		−0.004	−0.003		−0.002	−0.003
Magnetic anisotropy									
$E_a(electr.)$		0.10(0.20)			0.25(0.60)			0.10(0.25)	
$E_a(dipole)$		−0.21			−0.34			−0.38	
$E_a=E_a(electr.)+E_a(dipole)$		−0.11			−0.09			−0.28	
Easy axis		∥			∥			∥	

	hcp Co ML on Pt(111)			fcc Fe ML on Pt(111)			hcp Fe ML on Pt(111)		
Magnetic moments	Scalar	⊥	∥	Scalar	⊥	∥	Scalar	⊥	∥
μ_S (Co/Fe)	2.028	2.022	2.022	3.004	2.987	2.990	3.018	3.002	3.005
μ_S (Pt_1)	0.394	0.362	0.363	0.283	0.261	0.264	0.340	0.302	0.299
μ_S (Pt_2)	0.136	0.099	0.112	−0.030	−0.012	−0.005	0.106	0.052	0.068
μ_S (Pt_3)	0.037	0.021	0.032	−0.075	−0.045	−0.029	0.034	0.000	0.008
μ_S (Pt_4)	−0.006	−0.011	0.000	−0.081	−0.024	−0.013	0.003	−0.021	−0.018
μ_S (ΣPt)	0.428	0.424	0.513	0.204	0.088	0.136	0.447	0.272	0.335
μ_L (Co/Fe)		0.120	0.088		0.093	0.075		0.096	0.078
μ_L (Pt_1)		0.084	0.085		0.060	0.045		0.066	0.051
μ_L (Pt_2)		0.027	0.015		−0.008	−0.009		0.009	0.009
μ_L (Pt_3)		−0.004	0.004		−0.020	−0.005		−0.007	−0.001
μ_L (Pt_4)		−0.003	0.000		−0.003	−0.002		−0.004	
μ_L (ΣPt)		0.095	0.106		0.011	0.012		0.053	0.050
Magnetic anisotropy									
$E_a(electr.)$		0.62(1.10)			−0.59(−0.53)			−0.52(−0.40)	
$E_a(dipole)$		−0.19			−0.38			−0.38	
$E_a=E_a(electr.)+E_a(dipole)$		0.43			−0.97			−0.90	
Easy axis		⊥			∥			∥	

atom, i.e., the lower spin magnetic moment of the Co atoms on the Rh surface is compensated by a larger induced moment. The effective spin moment is essentially the same in the scalar-relativistic and fully relativistic calculations. The modest effective moment of the atoms in a Co ML is in contrast to the magnetization induced by isolated adatoms where larger effective moment of about 5 μ_B and 2.9 μ_B per Co atom on Pt(111) and Rh(111) surfaces have been calculated and found to be in good agreement with experiment.[21,71] In contrast to Co, no enhanced effective moment is found for a Fe ML on Rh(111) while on Pt(111) a larger effective moment of 3.47 μ_B/Fe atom is calculated.

Again for Fe, the effective moment of an isolated adatom is larger than for an atom in a compact monolayer.

(iv) The induced orbital moments in the top layer are larger in the Pt(111) substrate where we find $\mu_L = 0.084/0.085\ \mu_B$ for perpendicular/in-plane magnetization for hcp Co/Pt(111) and $\mu_L = 0.060/0.045\ \mu_B$ for fcc Fe/Pt(111). This last example also shows that the adsorption site causes only a small change in the induced orbital moments. Smaller induced orbital moments are found for Co/Rh(111), $\mu_L = 0.023\ \mu_B$ and isotropic, for Fe/Rh(111) all induced moments orbital moments are below $0.01\ \mu_B$.

(v) For a 2 ML Co/Rh(111) film, the Co spin moments in the top and interface layers are slightly reduced, but the spin moment induced on the topmost Rh layer is reduced by 50% compared to the monolayer [$\mu_S(\mathrm{Rh}_1) = 0.255/0.257$ against $0.524/0.524\ \mu_B$ for perpendicular and in-plane magnetization]. This is due to the higher local coordination of the Rh layer, which increases the local *d*-band width and thus reduces the induced moment. A previous study of a Co monolayer buried in a Rh(111) bulk[36] has shown that in absence of any surface-induced magnetic enhancement, a similar induced spin moment of $0.242\ \mu_B$ is found on the Rh layers directly binding to the Co monolayer. The orbital moment of the Co atoms at the free surface is almost unchanged while that of the interface layer is slightly reduced. The induced orbital moments below a bilayer are very small.

3. Magnetic anisotropy

It is well known that the calculation of the small magnetic anisotropy energy is hampered by serious convergence difficulties. Therefore for hcp Co/Rh(111) (where we found the smallest MAE) we have investigated how far the results are affected by modifying the slab thickness or the density of the *k*-point mesh. While the magnetic moments remain almost unchanged (as illustrated, for this example, in Fig. 9 for the spin moments), the MAE appears to be a more critical issue: (i) after decreasing the slab thickness from 11 to 8 and 5 Rh layers, we found a MAE of 0.15 meV/Co atom instead of 0.22 meV/Co atom, provided we increase the density of *k* points in consequence from a $12\times12\times1$ to a $12\times12\times2$ to conserve the same spacing between grid points in the Brillouin zone. With a coarser $12\times12\times1$ grid we find a MAE of 3.76 and 5.68 meV/Co atom for 8- and 5-layer slabs. Increasing the slab thickness from 11 to 14 Rh layers while keeping a *k*-point mesh of $12\times12\times1$, reduces the MAE to 0.10 meV/Co atom. This indicates that the spurious moments induced at the bottom layers have only a limited influence on the MAE and that a 11-layer-thick slab is sufficient to get a well-converged MAE. (ii) On the other hand, increasing the density of the *k*-point mesh $N\times N\times1$ from $N=12$ to $N=14$, 16, and 18 (for the same 11-layer-thick slab as substrate model), the MAE is found to vary from 0.22 meV/atom to 0.16 meV/atom, 0.20 meV/atom, and 0.11 meV/atom, respectively. The results summarized in Fig. 10 demonstrate that our computational setup allows to get MAE converged within 0.1 meV/Co atom.

It is remarkable that except for Fe/Rh(111) in all cases the sign of the MAE of the supported and free-standing MLs is different. For hcp Co/Pt(111) we calculate an electronic contribution of $E_a(electr.) = +0.62(-1.65)$ meV/atom (the value in parentheses refers to the strained free-standing monolayer matching the substrate), for fcc Fe/Pt(111) we find $E_a(electr.) = -0.59(+0.60)$ meV/atom, and almost the same value of $E_a(electr.) = -0.52$ meV/atom for a ML with the Fe atoms in the hcp hollows. For MLs on a Rh substrate we find $E_a(electr.) = +0.10(-1.22)$ meV/atom for the Co and $E_a(electr.) = +0.1(+0.50)$ meV/atom for the Fe ML. For a Co bilayer on Rh(111), the positive MAE is slightly enhanced. The dipolar contributions are always negative, hence the tendency to in-plane anisotropy of the Fe films is enhanced whereas the perpendicular MAE of Co/Pt(111) is reduced. For Co monolayer and bilayer on Rh(111) the dipolar contribution even overrules the electronic MAE, resulting in a very modest in-plane anisotropy. However, it has to be emphasized that in these cases the modest size of the MAE is close to the computational accuracy.

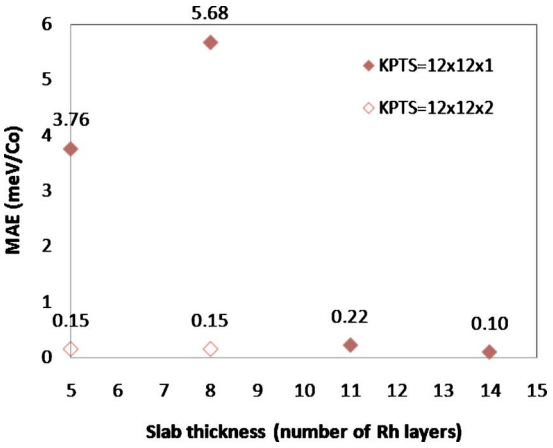

FIG. 10. (Color online) Convergence of the band contribution to the MAE of a Co/Rh(111) adlayer with respect to the thickness of the Rh slab, as calculated using two different Brillouin-zone meshes, cf. text.

If the MAE is calculated using the magnetic force theorem and the total electronic DOS for perpendicular and in-plane magnetization, calculated with the frozen potential from converged out-of-plane calculations, semiquantitative agreement with the total-energy differences is achieved. For a Co ML on both substrates the force theorem leads to a MAE increased by about a factor of 2, for the supported Fe MLs agreement is even slightly better. Still, the force theorem is found to be very useful in elucidating the surprising reversal of the sign of the MAE in supported compared to free MLs. For a Co bilayer on Rh(111) the electronic contribution to the MAE favoring out-of-plane magnetization is nearly doubled but because of a corresponding increase in the dipolar term favoring an in-plane easy axis the total MAE remains unchanged.

4. Electronic origin of the MAE of supported MLs

The comparison of the MAE for supported and free-standing MLs raises some interesting questions: (i) in three out of four cases the sign of the MAE is reversed due to the interaction with the substrate. (ii) The coupling of the strongly ferromagnetic adlayer to a nonmagnetic polarizable

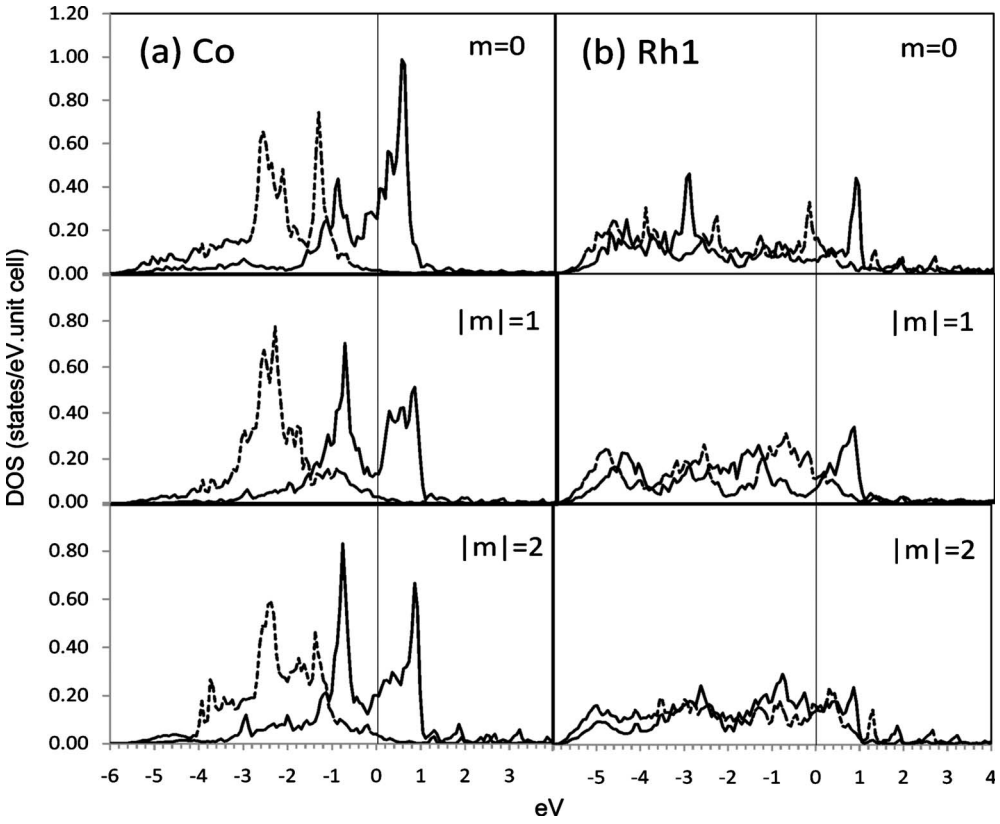

FIG. 11. Majority-spin (dashed lines) and minority-spin (solid lines) orbital-projected *d*-electron density of states for a Co monolayer on Rh(111) and for the top layer of the substrate.

substrate with a strong SOC does not increase the magnitude of the MAE. (iii) For both Co and Fe MLs on Rh(111) substrates, the absolute value of the MAE is dramatically reduced compared to the free-standing monolayers. For Co/Rh(111) the sign change and reduction in the MAE parallels corresponding changes in the orbital anisotropy while for Fe/Rh(111) the changes in the orbital moment is only rather modest. (iv) For Co and Fe MLs on Pt(111) the absolute value of the MAE is reduced only by a factor of 2 (Co) or remains almost unchanged (Fe) but the sign is reversed. An explanation of these surprising results must be sought in the electronic structure of the adlayer/substrate complexes. We shall discuss first the case of the Rh-supported MLs.

Figures 11 and 12 show the spin-polarized partial DOS of the magnetic adlayer and the first substrate layer of Co(Fe)/Rh(111). Compared to the free-standing MLs, the bandwidth of the $m=0, \pm 1$ states extending perpendicular to the layer are broadened due to the interaction with the substrate. The $m=0$ band which has almost nonbonding character in the free ML now displays a strong bonding-antibonding splitting. The exchange splitting is reduced. This effect is more pronounced for the Co ML such that majority and minority bands overlap. For the Rh substrate the exchange splitting induced by the interaction with the adlayer is most pronounced for the $m= \pm 1$ states and almost absent for $m = \pm 2$. The force theorem and the layer-decomposed DOS allow to separate the electronic contributions to the MAE coming from the magnetic layer and the substrate. For Co/Rh(111) these contributions are −0.002 meV/atom (Co), +0.09 meV/atom (first Rh layer), +0.04 meV/atom (second Rh layer), and +0.05 meV/atom (third Rh layer), together 0.18 meV/atom, to be compared to a total MAE of 0.10 meV/atom (TE) or 0.2 meV/atom (FT). For Fe/Rh(111) the corresponding layer-resolved contributions are 0.03, 0.19, 0.04, and 0.03 meV/atom, together 0.29 meV/atom to be compared to a total MAE of 0.10 meV/atom (TE) [0.25 meV/atom (FT)]. In both cases the contributions from the fourth substrate layer onward are $\leq$0.01 meV/atom.

Figure 13 shows the layer-decomposed changes $\Delta n^i(E)$ in the DOS induced by the change in the magnetization direction, as well as the layer-decomposed integrated contributions to the MAE, as calculated for Co/Rh(111). The analysis demonstrates that there are substantial changes in the layer-resolved DOSs even at higher binding energies and these changes gradually add to form a small contribution to the MAE. The situation is the same for Fe/Rh(111).

Hence the small positive electronic MAE for Co/Rh(111) results from an almost vanishing contribution from the adlayer and a dominant positive contribution from the substrate. The very small contribution of the adlayer parallels the strongly reduced, almost isotropic orbital magnetic moments. In this case the negative dipolar MAE is large enough such that the total MAE semiquantitatively agrees with experiment. For Fe/Rh(111) the electronic contribution to the MAE is also dominated by the substrate. Although both magnetic adlayer and substrate yield slightly larger positive values, the total is not large enough to outweigh the negative dipolar MAE and to achieve agreement with experiment.

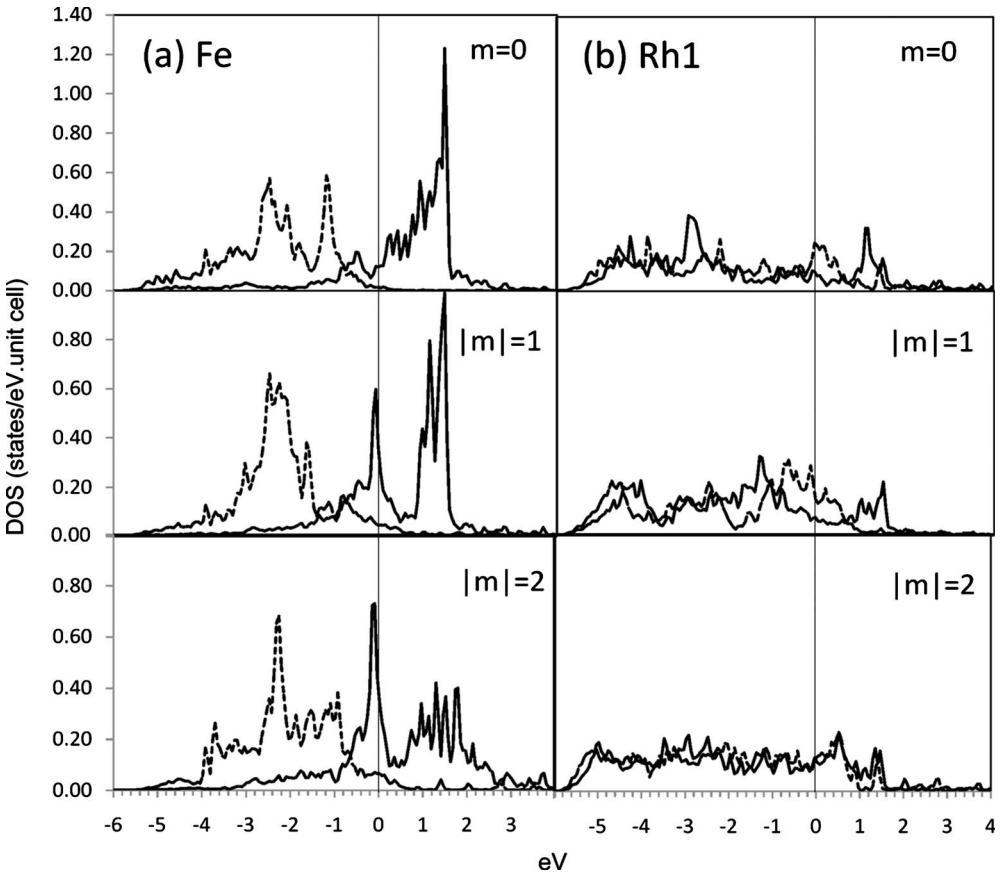

FIG. 12. Majority-spin (dashed lines) and minority-spin (solid lines) orbital-projected *d*-electron density of states for a Fe monolayer on Rh(111) and for the top layer of the substrate.

Figures 14 and 15 show the angular momentum and layer-decomposed DOS for Co(Fe)/Pt(111). Compared to the MLs on the Rh substrate, the bandwidths of the magnetic adlayers are reduced, the exchange splitting is increased. Examination of the $\Delta n_m^i(E)$ demonstrates that the orbital anisotropy of Co/Pt(111) is again dominated by the $m=\pm 1$ orbitals (although changed in sign and strongly reduced compared to the free-standing Co ML). The layer-resolved contributions to the MAE are 0.20 meV/atom from the Co and 0.94/0.16/0.09 meV/atom from the first/second/third Pt layer, together 1.39 meV/atom to be compared to a total MAE of 1.10 meV/atom (FT) or 0.62 meV/atom (TE). Hence the magnetic anisotropy is strongly dominated by the induced magnetization in the substrate with a strong SOC. For this system we have also analyzed the orbital-resolved contributions from the Co adlayer. In contrast to the free-standing ML where the negative contribution from the $m=\pm 1$ states dominates, for the supported ML all angular momentum states make small positive contributions (0.14/0.19/0.06 meV/atom for $m=0,\pm 1,\pm 2$).

The picture is different for Fe/Pt(111). For Fe in the fcc hollows the layer-resolved contributions to the MAE are −0.15/−0.01/−0.01/−0.04 meV/atom from the Fe and the top Pt layers, together −0.21 meV/atom (to be compared with a total MAE of −0.53 meV/atom (FT) or −0.59 meV/atom (TE). The orbital decomposition for the Fe layer yields −0.03/−0.15/−0.19 meV/atom (together −0.36 meV/atom) for the $m=0,\pm 1,\pm 2$ contributions. For Fe in the hcp hollows the contributions of the Fe and top Pt layer to the total MAE of −0.52(−0.40) meV/atom from TE (FT) are −0.4 meV/atom and −0.1 meV/atom, respectively. Admittedly, the details are somewhat affected by the uncertainties of the orbital-projections scheme and the smallness to the layer-resolved contributions but the main conclusions are still evident: in contrast to Co/Pt(111) for Fe/Pt(111) the leading contribution to the MAE still comes from the magnetic overlayer and not from the substrate.

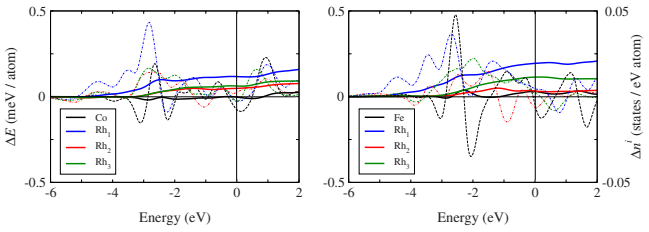

FIG. 13. (Color online) Changes $\Delta n^i(E)$ in the layer-decomposed densities of states with reorientation of the magnetization direction (dashed lines and left-hand scales) and integrated contributions to the MAE (full lines and right-hand scales) for supported (a) Co/Rh (111) MLs and (b) Fe MLs strained to match the Rh(111) surface, cf. text.

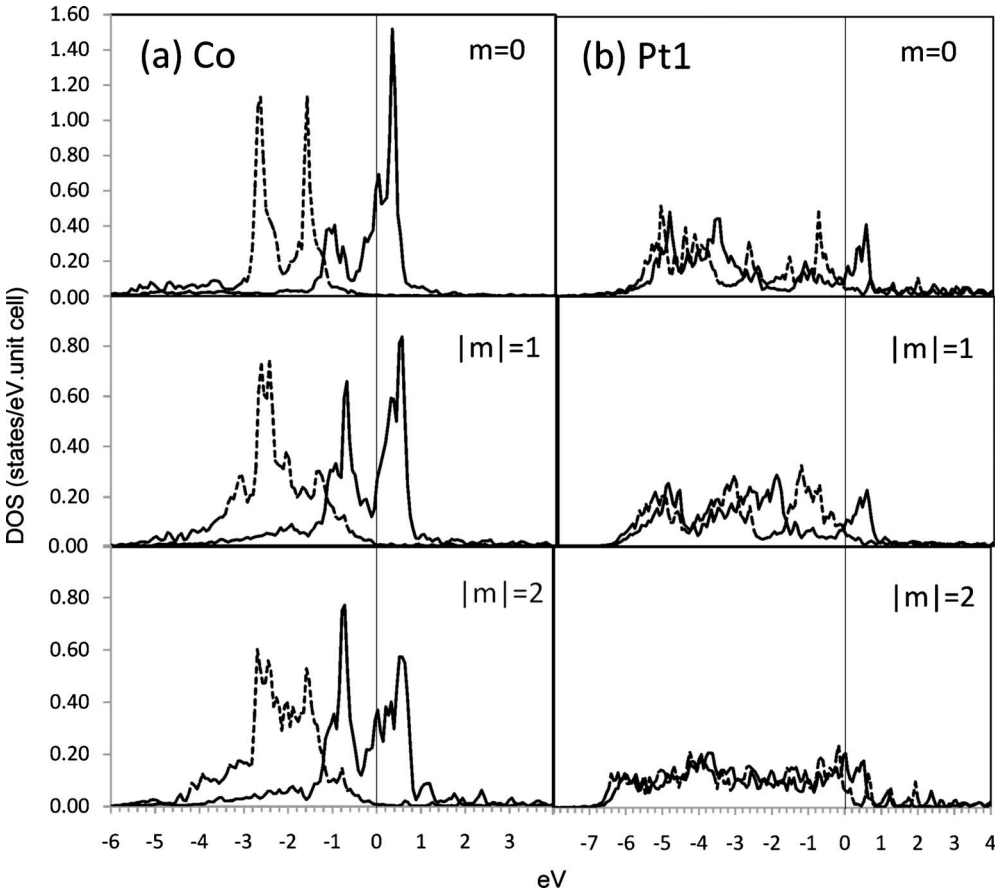

FIG. 14. Majority-spin (dashed lines) and minority-spin (solid lines) orbital-projected *d*-electron density of states for a Co monolayer on Pt(111) and for the top layer of the substrate.

5. Geometry and magnetic anisotropy

Necessarily, the calculated MAE depends on a number of unavoidable approximations. The motivation for our choice has been explained above but it is certainly interesting to examine whether different choices might lead to different results. This can be achieved through a comparison with the calculations of Moulas *et al.*[10] for Fe and Co monolayers on Pt(111). The methods and approximations used in these calculations are very different from ours: (i) screened Korringa-Kohn-Rostoker (SKKR) Green's-function calculations[83] on a semi-infinite substrate vs self-consistent DFT calculations in a plane-wave basis applied to a slab of finite thickness. (ii) Atomic-sphere approximation to the effective-potential vs full-potential approach. (iii) Local exchange-correlation functional vs semilocal gradient-corrected functional and (iv) adlayer continuing the bulklike structure of the substrate with experimental lattice constants vs fully relaxed adsorbate-substrate complex. (v) Adatoms always in fcc hollows vs adatoms in energetically optimal adsorption sites. (vi) MAE calculated nonself-consistently via the magnetic force theorem[84,85] vs MAE calculated from self-consistent total-energy differences,. To base the calculations on the Green's function of the clean, semi-infinite substrate instead on a slab of finite thickness might represent at first sight a definite advantage. However, the Dyson equation for the film-substrate complex is solved only for a finite number of near-surface layers which is much lower than the number of layers in our slabs (no information on the number of layers is given in the paper of Moulas *et al.* but values of induced moments are quoted only for four top layers). For our calculation we have demonstrated explicitly that convergence with respect to slab thickness has been achieved. Our results also permit the conclusion that the use of the force theorem leads to results which may be only semiquantitatively reliable. Our preceding comparative analysis of the magnetic anisotropy of isolated Co and Fe atom on Pt(111) has demonstrated that the choice of the exchange-correlation functional has only a minor influence on the MAE. Hence the decisive difference is the different description of the geometry of the adlayer/substrate complex.

The comparison of both approaches compiled in Table V demonstrates very good agreement for spin and orbital moments of the atoms in the supported films and their orbital anisotropies but significant differences in the induced moments and in the orbital anisotropies. The smaller induced spin and orbital moments from the SKKR calculations indicate a reduced adsorbate/substrate interaction because relaxation has been neglected, positioning the adlayer at a too large distance. Good agreement between both approaches is found for the contribution of the magnetic adlayer to the MAE. According to Moulas *et al.*[10] the contribution from the ML is 0.15 (0.20) meV/atom for Co and −0.10 (−0.15) meV/atom for Fe (our values are given in parenthe-

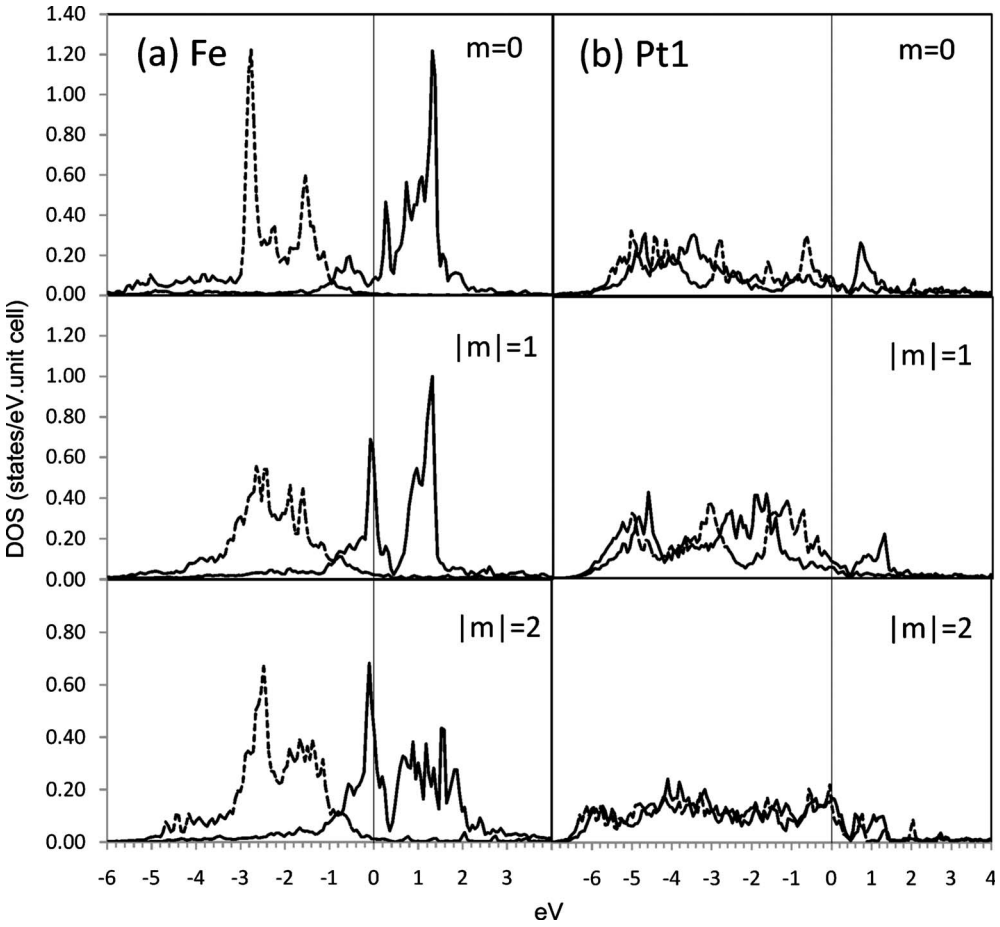

FIG. 15. Majority-spin (dashed lines) and minority-spin (solid lines) orbital-projected d-electron density of states for a Fe monolayer adsorbed in a fcc stacking sequence on Pt(111) and for the top layer of the substrate.

ses for comparison). In contrast, large discrepancies are found concerning the contributions from the substrate. In the SKKR calculations this is always negative, varying between −0.02 meV/atom for Co/Pt(111) to −0.6 meV/atom for Fe/Pt(111). In our calculation a large positive contribution from the Pt substrate dominates the MAE for Co/Pt(111). For Fe/Pt(111) we find a still negative but smaller negative contribution. Even bearing in mind that in our plane-wave approach the layer decomposition bears some uncertainty due to the projection on atomic spheres, these differences are important. For Co/Pt(111) the positive MAE derived from the SKKR calculations is so small that the negative contribution from the dipolar interactions prevails, whereas the larger substrate contribution from our calculation allows to achieve agreement with experiment. For Fe/Pt(111) no direct comparison with experiment is possible, in this case the XAS predicts only a low spin moment of 1.2 μ_B/atom, indicating that the Fe adlayer does not order ferromagnetically, but adopts some complex ferrimagnetic configuration similar to that recently reported for Ir(111).

VII. DISCUSSION AND CONCLUSIONS

The growth and the magnetic properties of Co and Fe monolayers on Rh(111) substrates have been investigated using scanning tunneling microscopy, x-ray absorption and magnetic circular dichroism spectroscopies, and magneto-optic Kerr effect. Low-temperature deposition leads to the formation of granular films which coalesce upon annealing at room temperature to form continuous monolayer films. STM experiments reveal for Co films a random network of dislocation lines separating fcc and hcp stacking regions while in Fe/Rh(111) films no dislocation lines are observed. This result is surprising, because the lattice mismatch with Rh is slightly larger for Fe than for Co, but it parallels similar observations for Co and Fe monolayers grown on Pt(111) substrates.[10] XMCD experiments at the $L_{2,3}$ edges of Co and Fe allow to determine the spin and orbital moments of the magnetic adlayers. For Co/Rh(111) both spin and orbital moments are found to be slightly enhanced compared to films grown on Pt(111). In contrast, Fe MLs have strikingly different magnetic properties if grown on close-packed Rh and Pt surfaces: films grown on Rh(111) show a spin moment of 2.76 μ_B strongly enhanced over the value in bulk Fe while for films grown on Pt(111) a low spin moment of 1.2 μ_B has been reported. The low average Fe spin moment has been tentatively attributed to the formation of a complex, noncollinear, and partially antiferromagnetic magnetic order similar to that recently reported for Fe/Ir(111).[43] The observation of a reduced Fe moment in pseudomorphic Fe/Pt(111) also correlates with the observation that in pseudomorphic Co films

TABLE V. Spin and orbital moments (μ_S and μ_L), orbital anisotropy ($\Delta\mu_L=\mu_L^{\perp}-\mu_L^{\parallel}$) (in μ_B) and MAE (in meV/atom) for Co/Pt(111) and Fe/Pt(111) calculated using the SKKR approach (Ref. 10) and in the present work (PW), using the total-energy (TE) differences or the magnetic force theorem (FT), cf. text.

	Co/Pt(111)		Fe/Pt(111)	
	SKKR	PW	SKKR	PW
μ_S (Co/Fe)	2.00	2.02	3.00	2.99
μ_L (Co/Fe)	0.15	0.120	0.09	0.093
$\Delta\mu_L$ (Co/Fe)	0.03	0.032	0.02	0.018
$\mu_S(\mathrm{Pt}_1)$	0.23	0.362	0.19	0.261
$\mu_L(\mathrm{Pt}_1)$	0.05	0.084	0.04	0.060
$\Delta\mu_L(\mathrm{Pt}_1)$		−0.001		0.015
MAE $E_a(electr.)$ FT total	+0.13	+1.10	−0.70	−0.53
MAE $E_a(electr.)$ FT-Co(Fe)	+0.15	+0.20	−0.10	−0.15
MAE $E_a(electr.)$ FT-Pt	−0.02	+1.19	−0.60	−0.06
MAE $E_a(electr.)$ TE		+0.62		−0.59

grown on W(110) the tendency toward ferromagnetic ordering is strongly reduced while it is preserved in reconstructed films with partial misfit dislocations.[86] XMCD spectra have also been measured at the $M_{2,3}$ edges of Rh. They allow to conclude that the magnetic moments induced in the substrate are ferromagnetically aligned with those in the magnetic adlayer but a quantitative determination of the induced magnetization was impossible. MOKE experiments show that granular Fe/Rh(111) films show superparamagnetic behavior while annealed continuous films display long-range ferromagnetic order with an out-of-plane easy axis. Both granular and continuous Co/Rh(111) films are ferromagnetic with an in-plane easy axis of magnetization, contrasting the perpendicular anisotropy of Co/Pt(111). The MAE has been calculated from the saturated magnetization curves, $E_a=-0.37\pm0.05$ meV/atom for Co/Rh(111) and $E_a=0.08\pm0.01$ meV/atom for Fe/Rh(111). This means that while for the Co ML the sign of the MAE is reversed compared to a ML on a Pt(111) support, for a Fe ML the sign remains the same.

Ab initio spin-polarized density-functional calculations including spin-orbit coupling have been performed for free-standing triangular Fe and Co monolayers and for monolayer films supported on both substrates. The free MLs have been studied with the aim to create a reference and to elucidate the physical mechanism determining the magnetic anisotropy of the supported films. A Co ML has a strongly enhanced isotropic spin moment, a substantial and strongly anisotropy orbital moment, and a large negative MAE. If the lattice constant in the ML is strained to match the Rh or Pt surfaces, spin moment, orbital anisotropy, and MAE increase, the MAE reaches even a value of −1.86 meV/atom in a film matching Pt(111). In comparison a Fe ML also shows a strongly enhanced spin moment, a modest and only weakly anisotropic orbital moment, and a smaller positive electronic contribution to the MAE. In strained MLs the positive MAE decreases but remains large enough to overcompensate the negative dipolar MAE. A detailed analysis of the orbital-decomposed contributions to the MAE allows to assign the difference in the sign to the electronic structure of the films. For Fe MLs the dominant contribution to the positive MAE arises from the splitting of the $m=\pm2$ states close to the Fermi level for perpendicular magnetization, for Co MLs the negative MAE is due to the off-diagonal coupling between the occupied $m=\pm1$ (odd) and the empty $m=0$ (even) minority-spin orbitals.

For the supported monolayers, unlike most previous investigations of the magnetic anisotropy energy the calculations have been performed for relaxed geometries of the adsorbate/substrate complex preserving the pseudomorphic relationship. The relaxation leads to an inward relaxation of the magnetic adlayer by about 10% compared to the ideal interlayer distance in the substrate and hence to an increased hybridization at the interface. The most important results from both theory and experiment are confronted in Table VI. Good agreement is found for the spin moments in the magnetic adlayer which are strongly enhanced compared to the bulk metals, except for Fe/Pt(111) where the exceptionally low spin moment of 1.2 μ_B was tentatively assigned to a complex magnetic structure with a substantial antiferromagnetic component. However, we have included the results calculated for a ferromagnetic Fe/Pt(111) ML for comparison with Fe/Rh(111) whose ferromagnetic order is confirmed by a large spin moment. While the experiments yield substantial orbital moments for both Co/Rh(111) and Fe/Rh(111) which are even slightly larger than on a Pt(111) substrate, the density-functional calculations predict orbital moments which are lower by a factor of 1.5–2.8 than the experimental

TABLE VI. Spin and orbital magnetic moment (μ_S and μ_L), both in μ_B/atom and magnetic anisotropy energy E_a (in meV/magnetic atom, a positive sign stands for perpendicular anisotropy) for Co and Fe monolayers on Rh(111) and Pt(111) substrates, comparison of theory and experiment. The experimental results for Pt(111) substrates are from Moulas *et al.*, Ref. 10.

	μ_S		μ_L		E_a	
	Expt.	Theor.	Expt.	Theor.	Expt.	Theor.
Co/Rh(111)	1.97 ± 0.08	1.96	0.34 ± 0.06	0.12	-0.37 ± 0.05	−0.11
Fe/Rh(111)	2.76 ± 0.16	2.82	0.21 ± 0.04	0.09	$\geq0.08\pm0.01$	−0.28
Co/Pt(111)	1.8 ± 0.1	2.02	0.31 ± 0.06	0.12	0.15 ± 0.02	0.43
Fe/Pt(111)	1.2 ± 0.4	2.99	0.14 ± 0.02	0.09	0.1 ± 0.05	−0.97

values and nearly isotropic. The quenching of the orbital moments is a consequence of the strong hybridization of adsorbate and substrate orbitals but a comparison with previous calculations based on an unrelaxed geometry shows that it is hardly influenced by the inward relaxation of the magnetic adlayer (in contrast to the case of isolated adatom). However, the inward relaxation leads to the formation of larger induced spin and orbital moments in the top layers of the substrate. For Co the induced spin moments are larger in Rh than in Pt substrates while Fe induces to a larger spin polarization of Pt than Rh. The induced orbital moments are much larger in the Pt substrate for both adlayers, reflecting the stronger spin-orbit coupling.

The magnetic anisotropy of the supported monolayers is entirely different from that of the free MLs. For Co MLs on both substrates we calculate a modest positive electronic contribution to the MAE. For Co/Pt(111) the value is large enough to result in a perpendicular MAE after adding the negative dipolar contribution while for Co/Rh(111) the dipolar term determines the in-plane MAE. In both cases theory and experiment are in good agreement. For Fe/Rh(111) we find a small positive electronic contribution to the MAE and a larger negative one for Fe/Pt(111). After adding the dipolar term, an in-plane MAE is predicted in contrast to experiment for both systems. For Fe MLs on Pt we have also investigated both fcc and hcp stacking sequences of the adlayer. In contrast to the case of isolated adatoms, only a modest site dependence of the magnetic properties of the adsorbed monolayers has been found.

The magnetic force theorem has been used to estimate the adlayer and substrate contributions to the MAE. Supported Co MLs make only a minimal contribution to the MAE (this correlates to the strongly reduced orbital anisotropy), a small positive contribution comes from the Rh, a much larger, equally positive contribution from the Pt substrate. For supported Fe MLs on Rh the positive MAE arises again from the substrate, but it is not large enough to outweigh the dipolar term, for Fe MLs on Pt both adlayer and substrate make about equal negative contributions to the MAE. We also note that while for the free-standing MLs the MAE is strongly dominated by orbitals of a well-defined parity ($m=\pm 1$ for Co, $m=\pm 2$ for Fe MLs), the contributions of all d states are of comparable size for supported MLs.

For multilayer films the experiments show for Co/Rh(111) a change from in-plane to perpendicular anisotropy in a bilayer and back to in plane for a film with three monolayers. The calculations show that the electronic contribution to the MAE is more than twice as large for the bilayer than for a monolayer but this increase is just not large enough to overcompensate a more modest increase in the negative dipolar contribution. The central problem of any theory of the magnetic anisotropy of these systems remains, however, to find a correct model for the geometric and magnetic structures of ultrathin Fe films on these substrates.

ACKNOWLEDGMENTS

The calculations described in this paper were performed using HPC resources from GENCI-CINES (Grant No. 2009-x2009095045) at the CINES (Montpellier, France) and from the Vienna Scientific Cluster (VSC). Financial support from the Swiss National Science Foundation under Grants No. 200020-109800 and No. 200020-112322, the Spanish Ministerio de Ciencia e Innovación (Grant No. MAT2007-62341), the Catalan Agència de Gestió d'Ajuts Universitaris i de Recerca (2009 SGR 695), and from the European Science Foundation EUROCORES 05-SONS-FP-009 SANMAG are gratefully acknowledged.

[1] D. Sellmyer and R. Skomski, *Advanced Magnetic Nanostructures* (Springer, New York, 2006).
[2] *The Physics of Ultra-High-Density Magnetic Recording*, Springer Series in Surface Science Vol. 41, edited by M. L. Plumer, J. van Ek, and D. Weller (Springer, Berlin, 2001).
[3] N. Weiss, T. Cren, M. Epple, S. Rusponi, G. Baudot, S. Rohart, A. Tejda, V. Repain, S. Rousset, P. Ohresser, F. Scheurer, P. Bencok, and H. Brune, Phys. Rev. Lett. **95**, 157204 (2005).
[4] H. Brune and P. Gambardella, Surf. Sci. **603**, 1812 (2009).
[5] P. Gambardella, S. Rusponi, M. Veronese, S. S. Dhesi, C. Grazioli, A. Dallmeyer, I. Cabria, R. Zeller, P. H. Dederichs, K. Kern, C. Carbone, and H. Brune, Science **300**, 1130 (2003).
[6] P. Gambardella, M. Blanc, L. Bürgi, K. Kuhnke, and K. Kern, Surf. Sci. **449**, 93 (2000).
[7] P. Gambardella, A. Dallmeyer, K. Maiti, M. C. Malagoli, W. Eberhardt, K. Kern, and C. Carbone, Nature (London) **416**, 301 (2002).
[8] P. Gambardella, A. Dallmeyer, K. Maiti, M. C. Malagoli, S. Rusponi, P. Ohresser, W. Eberhardt, C. Carbone, and K. Kern, Phys. Rev. Lett. **93**, 077203 (2004).
[9] D. Repetto, T. Y. Lee, S. Rusponi, J. Honolka, K. Kuhnke, V. Sessi, U. Starke, H. Brune, P. Gambardella, C. Carbone, A. Enders, and K. Kern, Phys. Rev. B **74**, 054408 (2006).
[10] G. Moulas, A. Lehnert, S. Rusponi, J. Zabloudil, C. Etz, S. Ouazi, M. Etzkorn, P. Bencok, P. Gambardella, P. Weinberger, and H. Brune, Phys. Rev. B **78**, 214424 (2008).
[11] M. Komelj, C. Ederer, J. W. Davenport, and M. Fähnle, Phys. Rev. B **66**, 140407 (2002).
[12] S. Gallego, L. Szunyogh, P. Weinberger, and M. C. Munoz, Phys. Rev. B **69**, 224408 (2004).
[13] A. B. Shick, F. Máca, and P. M. Oppeneer, J. Magn. Magn. Mater. **290-291**, 257 (2005).
[14] J. Dorantes-Dávila and G. M. Pastor, Phys. Rev. B **72**, 085427 (2005).
[15] M. Komelj, D. Steiauf, and M. Fähnle, Phys. Rev. B **73**, 134428 (2006).
[16] M. Tsujikawa, A. Hosokawa, and T. Oda, J. Phys.: Condens. Matter **19**, 365208 (2007).
[17] C. Etz, J. Zabloudil, P. Weinberger, and E. Y. Vedmedenko, Phys. Rev. B **77**, 184425 (2008).
[18] M. Tsujikawa, A. Hosokawa, and T. Oda, Phys. Rev. B **77**, 054413 (2008).

[19] A. Mosca Conte, S. Fabris, and S. Baroni, Phys. Rev. B **78**, 014416 (2008).
[20] M. Tsujikawa and T. Oda, Phys. Rev. Lett. **102**, 247203 (2009).
[21] P. Błoński and J. Hafner, J. Phys.: Condens. Matter **21**, 426001 (2009).
[22] R. Robles, J. Izquierdo, and A. Vega, Phys. Rev. B **61**, 6848 (2000).
[23] J. W. Lee, J. R. Jeong, S. Ch. Shin, J. Kim, and S. K. Kim, Phys. Rev. B **66**, 172409 (2002).
[24] M. Sawada, K. Hayashi, and A. Kakizaki, J. Phys. Soc. Jpn. **72**, 1161 (2003).
[25] T. Yokoyama, D. Matsumura, K. Amemiya, S. Kitagawa, N. Suzuki, and T. Ohta, J. Phys.: Condens. Matter **15**, S537 (2003).
[26] M. Przybylski, L. Yan, J. Zukrowski, M. Nyvlt, Y. Shi, A. Winkelmann, J. Barthel, M. Waśniowska, and J. Kirschner, Phys. Rev. B **73**, 085413 (2006).
[27] B. V. Reddy, S. N. Khanna, and B. I. Dunlap, Phys. Rev. Lett. **70**, 3323 (1993).
[28] T. Futschek, M. Marsman, and J. Hafner, J. Phys.: Condens. Matter **17**, 5927 (2005).
[29] O. Eriksson, R. C. Albers, and A. M. Boring, Phys. Rev. Lett. **66**, 1350 (1991).
[30] S. Blügel, Phys. Rev. Lett. **68**, 851 (1992).
[31] A. J. Cox, J. G. Louderback, and L. A. Bloomfield, Phys. Rev. Lett. **71**, 923 (1993).
[32] T. Shinohara, T. Sato, and T. Taniyama, Phys. Rev. Lett. **91**, 197201 (2003).
[33] G. G. Low and T. M. Holden, Proc. Phys. Soc. London **89**, 119 (1966).
[34] T. Herrmannsdörfer, S. Rehmann, W. Wendler, and F. Pobell, J. Low Temp. Phys. **104**, 49 (1996).
[35] S. Mitani, K. Takahashi, M. Sano, H. Fujimori, A. Osawa, and H. Nakajima, J. Magn. Magn. Mater. **148**, 163 (1995).
[36] S. Dennler, J. Hafner, M. Marsman, and J. Morillo, Phys. Rev. B **71**, 094433 (2005).
[37] M. A. Tomaz, D. C. Ingram, G. R. Harp, D. Lederman, E. Mayo, and W. L. O'Brien, Phys. Rev. B **56**, 5474 (1997).
[38] M. A. Tomaz, E. Mayo, D. Lederman, E. Hallin, T. K. Sham, W. L. O'Brien, and G. R. Harp, Phys. Rev. B **58**, 11493 (1998).
[39] K. Hayashi, M. Sawada, A. Harasawa, A. Kimura, and A. Kakizaki, Phys. Rev. B **64**, 054417 (2001).
[40] K. Hayashi, M. Sawada, H. Yamagami, A. Kimura, and A. Kakizaki, Physica B **351**, 324 (2004).
[41] D. Spišák and J. Hafner, Phys. Rev. B **73**, 155428 (2006).
[42] G. Ju, J. Hohlfeld, B. Bergman, R. J. M. van de Veerdonk, O. N. Mryasov, J.-Y. Kim, X. Wu, D. Weller, and B. Koopmans, Phys. Rev. Lett. **93**, 197403 (2004).
[43] K. von Bergmann, S. Heinze, M. Bode, E. Y. Vedmedenko, G. Bihlmayer, S. Blügel, and R. Wiesendanger, Phys. Rev. Lett. **96**, 167203 (2006).
[44] D. Pescia, G. Zampieri, M. Stampanoni, G. L. Bona, R. F. Willis, and F. Meier, Phys. Rev. Lett. **58**, 933 (1987).
[45] H. Tokano, H. Yanagihara, and E. Kita, J. Appl. Phys. **97**, 016103 (2005).
[46] F. El Gabaly, S. Gallego, C. Muñoz, L. Szunyogh, P. Weinberger, C. Klein, A. K. Schmid, K. F. McCarty, and J. de la Figuera, Phys. Rev. Lett. **96**, 147202 (2006).
[47] A. Lehnert, P. Buluschek, N. Weiss, J. Giesecke, M. Treier, S. Rusponi, and H. Brune, Rev. Sci. Instrum. **80**, 023902 (2009).
[48] B. T. Thole, P. Carra, F. Sette, and G. van der Laan, Phys. Rev. Lett. **68**, 1943 (1992).
[49] P. Carra, B. T. Thole, M. Altarelli, and X. Wang, Phys. Rev. Lett. **70**, 694 (1993).
[50] C. T. Chen, Y. U. Idzerda, H.-J. Lin, N. V. Smith, G. Meigs, E. Chaban, G. H. Ho, E. Pellegrin, and F. Sette, Phys. Rev. Lett. **75**, 152 (1995).
[51] D. Weller, J. Stöhr, R. Nakajima, A. Carl, M. G. Samant, C. Chappert, R. Mégy, P. Beauvillain, P. Veillet, and G. A. Held, Phys. Rev. Lett. **75**, 3752 (1995).
[52] R. Wu and A. J. Freeman, Phys. Rev. Lett. **73**, 1994 (1994).
[53] R. Nakajima, J. Stöhr, and Y. U. Idzerda, Phys. Rev. B **59**, 6421 (1999).
[54] J. W. Lee, J. R. Jeong, D. H. Kim, J. S. Ahn, J. Kim, and S. C. Shin, Rev. Sci. Instrum. **71**, 3801 (2000).
[55] R. M. Bozorth, Phys. Rev. **50**, 1076 (1936).
[56] H. Röder, K. Bromann, H. Brune, and K. Kern, Surf. Sci. **376**, 13 (1997).
[57] B. Holst, M. Nohlen, K. Wandelt, and W. Allison, Surf. Sci. **377-379**, 891 (1997).
[58] C. Günther, J. Vrijmoeth, R. Q. Hwang, and R. J. Behm, Phys. Rev. Lett. **74**, 754 (1995).
[59] F. E. Gabaly, J. M. Puerta, C. Klein, A. Saa, A. K. Schmid, K. F. McCarthy, J. I. Cerda, and J. de la Figuera, New J. Phys. **9**, 80 (2007).
[60] G. Kresse and J. Hafner, Phys. Rev. B **47**, 558 (1993).
[61] G. Kresse and J. Furthmüller, Phys. Rev. B **54**, 11169 (1996); Comput. Mater. Sci. **6**, 15 (1996).
[62] P. E. Blöchl, Phys. Rev. B **50**, 17953 (1994).
[63] G. Kresse and D. Joubert, Phys. Rev. B **59**, 1758 (1999).
[64] J. P. Perdew, J. A. Chevary, S. H. Vosko, K. A. Jackson, M. R. Pederson, D. J. Singh, and C. Fiolhais, Phys. Rev. B **46**, 6671 (1992).
[65] S. H. Vosko, L. Wilk, and M. Nusair, Can. J. Phys. **58**, 1200 (1980).
[66] J. P. Perdew, K. Burke, and M. Ernzerhof, Phys. Rev. Lett. **77**, 3865 (1996).
[67] E. G. Moroni, G. Kresse, J. Hafner, and J. Furthmüller, Phys. Rev. B **56**, 15629 (1997).
[68] G. Kresse and O. Lebacq, VASP manual, http://cms.mpi.univie.ac.at/vasp/
[69] D. Hobbs, G. Kresse, and J. Hafner, Phys. Rev. B **62**, 11556 (2000).
[70] M. Marsman and J. Hafner, Phys. Rev. B **66**, 224409 (2002).
[71] P. Błoński, A. Lehnert, S. Dennler, S. Rusponi, M. Etzkorn, G. Moulas, P. Bencok, P. Gambardella, H. Brune, and J. Hafner, Phys. Rev. B **81**, 104426 (2010).
[72] H. J. Monkhorst and J. D. Pack, Phys. Rev. B **13**, 5188 (1976).
[73] S. Hengrasmee, K. Mitchell, P. Watson, and J. White, Can. J. Phys. **58**, 200 (1980).
[74] N. Materer, U. Starke, A. Barbieri, R. Döll, K. Heinz, M. A. Van Hove, and G. A. Somorjai, Surf. Sci. **325**, 207 (1995).
[75] R. Wyckoff, *Crystal Structures* (Wiley, New York, London, 1963).
[76] S. C. C. Abrahams, L. Guttman, and J. S. Kasper, Phys. Rev. **127**, 2052 (1962).
[77] P. Bruno, Phys. Rev. B **39**, 865 (1989).
[78] G. H. O. Daalderop, P. J. Kelly, and M. F. H. Schuurmans, Phys. Rev. B **50**, 9989 (1994).
[79] P. Błoński and J. Hafner, Phys. Rev. B **79**, 224418 (2009).
[80] T. O. Strandberg, C. M. Canali, and A. H. MacDonald, Phys.

Rev. B **77**, 174416 (2008).
[81] A. Smogunov, A. Dal Corso, A. Delin, R. Weht, and E. Tosatti, Nat. Nanotechnol. **3**, 22 (2008); A. Smogunov, A. Dal Corso, and E. Tosatti, Phys. Rev. B **78**, 014423 (2008).
[82] J. Velev, R. F. Sabirianov, S. S. Jaswal, and E. Y. Tsymbal, Phys. Rev. Lett. **94**, 127203 (2005).
[83] L. Szunyogh, B. Újfalussy, P. Weinberger, and J. Kollár, Phys. Rev. B **49**, 2721 (1994).
[84] A. R. Mackintosh and O. K. Andersen, in *Electrons at the Fermi Surface*, edited by M. Springford (Cambridge University Press, London, 1980), Sec. 3.1.
[85] V. Heine, Solid State Phys. **35**, 114 (1980).
[86] N. N. Shukla and R. Prasad, Phys. Rev. B **70**, 014420 (2004).
[87] T. Cren, S. Rusponi, N. Weiss, M. Epple, and H. Brune, J. Phys. Chem. B **108**, 14685 (2004).